

A basic model for IVUS image simulation

*Misael Rosales*¹ and *Petia Radeva*²

¹Laboratorio de Física Aplicada, Facultad de Ciencias, Departamento de Física de la Universidad de los Andes Mérida/Venezuela

²Centre de Visió per Computador, Universidad Autònoma de Barcelona, Edifici O, Campus UAB, 08193 Bellaterra, Barcelona Spain

Contents

A basic model for IVUS image simulation	i
Introduction	2
0.1 Technical aspects of the IVUS	3
0.2 Present limitations of IVUS technique and a need of a generation model of IVUS data	6
A Basic IVUS Image Model.	9
0.3 Formal Definition of the Image Model	10
0.3.1 The ultrasound pulse	12
0.4 Principal features of IVUS data.	15
0.4.1 Image resolution	15
0.4.1.1 Axial resolution	15
0.4.1.2 Angular resolution	17
0.4.2 The beam intensity	19
0.4.3 Ultrasound beam sweeping criterion	20
0.4.4 Determining the scatterer number of arterial structures	22
0.5 Simulation of IVUS image	25
0.5.1 Generation of the simulated arterial structure	25
0.5.2 1D echogram generation	27
0.5.3 2D echogram generation	28
0.5.4 Final image processing	31
0.6 Validation of the image simulation model	31
0.6.1 Scatterer radial distribution	33
0.6.2 DBC distribution	34
0.6.3 IVUS image features	34
0.6.3.1 Spatial Resolution	34
0.6.3.2 Optimal Ultrasound Frequency	37
0.6.3.3 Optimal Attenuation Coefficient	37
0.6.3.4 The beam number influence	38

0.6.4	Real vs simulated IVUS	38
0.6.5	Polar images	41
Conclusions	55
0.7	Conclusions	55
Question and Answer	60
0.7.1	Questions	60
0.7.2	Answers	60

Introduction

The arteriosclerotic cardiovascular diseases [1] increase their incidence in vertiginous form, reaching after half-full of the decade of the fifties the first place like cause of mortality in the industrialized countries, place that at the moment occupies over the cancer and the accidents. In effect, the arteriosclerotic diseases, in general (infarct to miocardio, angina of chest, accidents cerebrovascular, and arterial diseases of the legs and arms) have caused, and continue causing, more deaths and consultations in the rooms of emergency and doctor's offices than any other disease in this century, including the AIDS. The coronary arterial diseases are developed due to a narrowing (stenosis) of the walls of the coronary arteries, caused by the accumulation of fibrotic material and calcium crystals [2]. The development of this type of plaque normally takes in humans between 15 and 20 years to form. There exist complicated injuries, which generate the formation of thrombus, the rupture of the plaque can be considered an important mechanism of the acute coronary syndromes. An imminent problem that happens if the arteries narrow too much due to the stenosis is that the blood flow diminishes in significant form. A total occlusion can take place by the maintained increase of a stenosis but also it can become serious due to a thrombosis. The result can be an infarct. The introduction in the field of the medical image of the **IntraVascular UltraSound (IVUS)** [3, 4] as an exploratory technique has made a significant change to the understanding of the arterial diseases and individual patterns of diseases in the coronary arteries. Although the coronary angiography [5, 6] provides with 2D information about the coronary anatomy, serving as guide in the operations, it is limited when not allowed to access to the mechanism of the disease, composition and extension of the same. On the contrary IVUS technique visualizes the cross-section (Fig. 1) of the artery allowing an evaluation of the plaque as well as of the different layers from the arterial wall. The IVUS image [2, 5, 6] provides qualitative (Fig. 2) information about:

The causes and severity of the narrowing of the arterial lumen, distinction

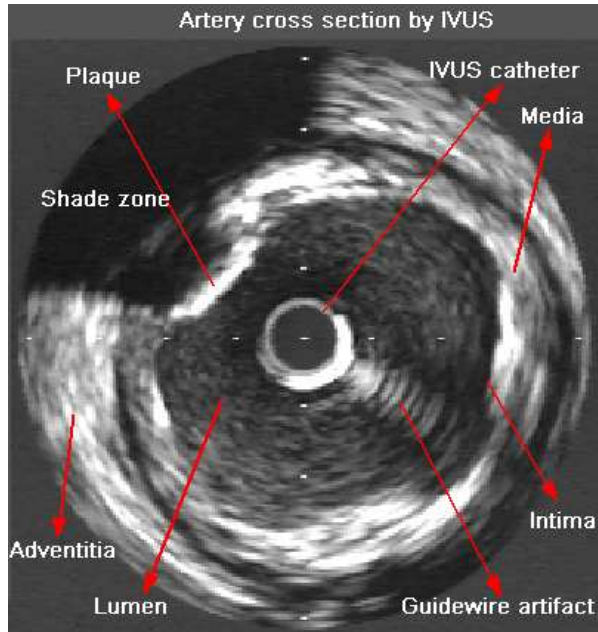


Figure 1: Typical 2D IVUS image indicating the location of the principal morphological arterial structures and artifacts.

of thrombus of the arteriosclerotic plaque, recognition of calcium deposits in the arterial wall, unexpected evaluation of the awaited changes and complications in the coronary arteries after an intervention as angioplasty, evaluation and diagnose of coronary arterial aneurysms, diagnose of fissures of arterial coronary plaques: determination and location, dimensions, type (eccentric and concentric) and composition of the arteriosclerotic plaque.

0.1 Technical aspects of the IVUS

The images of ultrasound [7] are based on the reception and transmission of the high frequency sound waves. The transmitted wave propagates through the material until striking the reflecting object. The reflected wave returns and is received by the transducer. The time between the transmission and the reception of the wave is directly related to the distance between the source and the reflector. The advantage of the ultrasound is that it can travel through the water and of the smooth tissue. Additionally, the ultrasound is inoffensive at

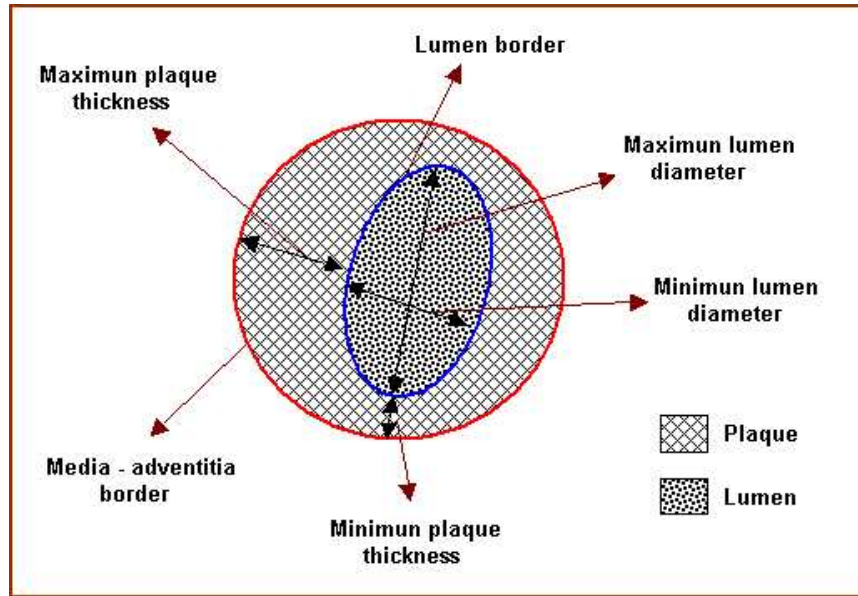


Figure 2: Geometric parameters of an artery that make possible to measure by means of Intravascular Ultrasound.

the used levels of energy for the generation of the image. A standard configuration of IVUS acquisition images consists of three components: Fig. 3 show a scheme of catheter with a piezoelectric transducer miniaturized, the pull-back unit and the console to reconstruct the images. IVUS catheter has a rank of measures that oscillates between 2,9 to 3,5 F (0,96 to 1,17 mm) of diameter. The quality of the image depends on the operation frequency, being this of the order of 20 to 50 Mhz, the lateral resolution is approximately of the order of $113 \mu m$ and the axial resolution is of the order of $80 \mu m$ [8]. The IVUS images acquisition process, is initiated when the catheter is manually (guided by the angiography) inserted within the artery (Fig. 3 (a)). The catheter pullback is made at linear constant velocity (usually 0.5 mm/s) and constant angular velocity of 1800 rev/min. The pivoting transducer sends a radially focused beam of ultrasound and receives its corresponding echoes. The obtained radial lines for different transducer angular positions are adequately processed, giving as a result a 2D cross section artery image (Fig. 3 (d)). The sequence can be shown as a longitudinal sequence, which gives a longitudinal artery cut (Fig. 3 (e)). The resolution of a ultrasound image is directly related to the ultrasound

signal frequency, high frequencies allow to obtain better resolution. Nevertheless, when increased the frequency, the attenuation of the waves of ultrasound increases while penetrating the biological tissue. The typical frequencies of the IVUS technique are in the rank of 20 to 50 MHz, with inferior resolutions of $50 \mu\text{m}$.

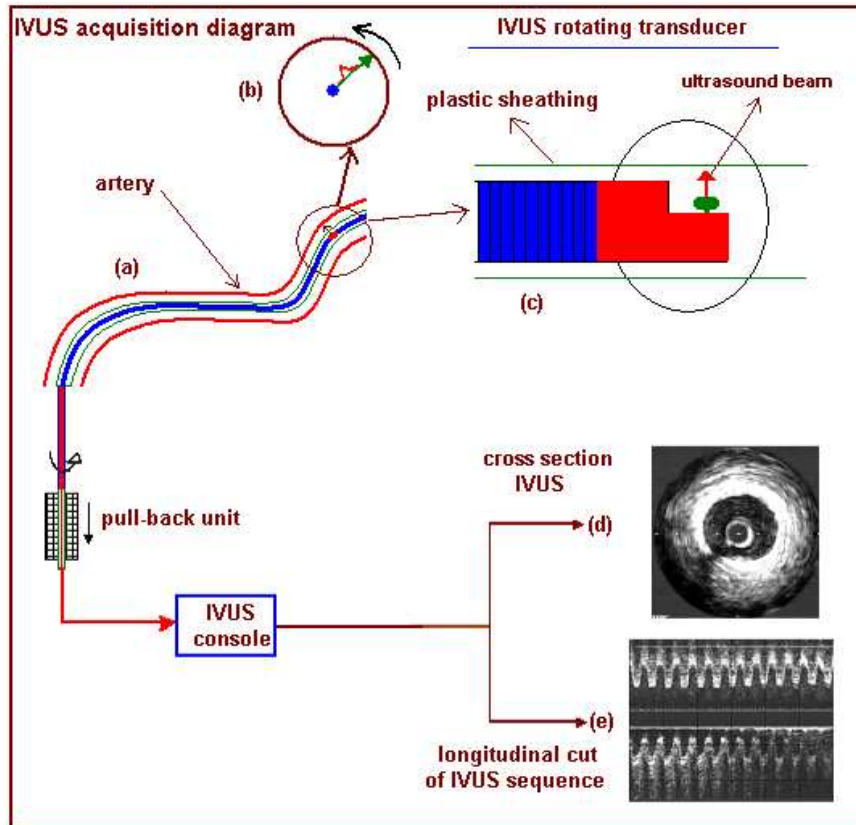


Figure 3: The IVUS catheter is manually positioned within the artery (a), it is extracted by a pullback unit at a constant linear velocity and rotated at a constant angular velocity. The information is transformed by the IVUS console as unique cross section artery grey levels image (d) or a longitudinal image sequence (e).

0.2 Present limitations of IVUS technique and a need of a generation model of IVUS data

The main roll of IVUS technique is to serve as a guide in the interventional procedures allowing to measure the cross-section of the artery. The precision in the measurements of distance is subject to the following potential sources of error [9]:

- a) Incorrect identification of the surface and the sections to be measured. Although the vessel and the interface defining the wall vessel have sufficiently good acoustic in most of the cases, still in several cases the identification of the surface and differentiating tissues can result difficult. When improving the radial resolution, it could improve the detection of contours, this would reduce the error. These errors can in some cases be systematic and lead to an overestimation of the dimensions. This could get considerably worse if the irregularities of the vessels are very pronounced.
- b) Assumption that the sound speed is constant in the arterial structure. The second kind of problem related to assuming the constant speed of the sound at 1540 m/seg, is systematic and small of the order of 1 to 2%, which brings as a consequence the propagation of the error to the location of each one of the structures in study.
- c) Artifacts caused by inhomogeneities in the rotation of the catheter and pronounced reverberations generated by very acute irregularities of the vessel. The appearance of some artifacts such as the inhomogeneities in the rotation of the catheter, has influences on the quality of the image. The absence of beams, when the catheter stops momentarily, brings as a consequence a propagation of errors in the tangential direction of the image.
- d) Presence of zones of acoustic shade which prevents to access certain regions of interest. The presence of zones of acoustic shade is intimately bound to the presence of calcification or regions of high acoustic impedance. The shades prevent that some structures can be evaluated from the distribution of the grey levels.
- e) The presence of the catheter, the reticule and the guide are troublesome for the processing of the images. The presence of the catheter, the reticule and the guide are quite uncomfortable when it is desired to evaluate the data by some procedure of images processing.

f) Impossibility to locate spatially the catheter. The impossibility to locate the catheter with respect to a specific axis of coordinates makes impossible any attempt of three-dimensional representation of the vessel only with IVUS technique. For example: spatial location of the effective section of the lumen and location of plaque and the reconstruction in the lengthwise direction of the vessel are still an open problem of investigation [9].

g) Impossibility to evaluate dynamic parameters, different from the single static characterization using the grey levels. First achievements are related to IVUS elastography [7] which purpose is to propose a technique for tissue characterization.

The mentioned shortcomings are difficult to quantify and depend on the experience of the operator that usually means he should have been trained by a large amount of patient cases. Some of the limitations of IVUS technique can be attenuated through algorithms of image processing; the limitations due to a suboptimal location of the borders of the arterial structure can be improved with new algorithms of segmentation. The question is how to develop robust algorithms that can solve these problems analyzing the artifacts with their multiple appearance in IVUS images. Having a complete set of patient data to present all variance of artifacts appearance in images would mean to dispose of a huge amount of patient cases. A more efficient solution is to develop a simulation model for IVUS data construction so that synthetic data are available in order to "train" image processing techniques. In this way, different appearance of artifacts can be designed to assure the robust performance of image processing techniques.

Differences in IVUS data are caused not only by different morphological structures of vessels but also by different parameters that influence the formation of IVUS images. The images depend on the IVUS apparatus calibration as well as interventional devices, small differences in parameters can lead to different grey-level appearance that can be interpreted in a different way by the physicians. Having a simulation model for IVUS data can help to the training of medical staff as well as can have an important role in designing and testing new interventional devices. At the end, being aware which parameters and in which grade influence to image formation is of unquestionable importance for all persons involved in comprehension of IVUS data and taking final decision for diagnosis and intervention of vessel lesions. In this chapter, we discuss a simple

simulation model for formation of 2D IVUS data that explains the complete process of data generation as a result of the interaction between ultrasound signals and vessel morphological structures.

A Basic IVUS Image Model

Correct image processing needs of understanding image formation, grey level meaning, artifact causes, the averaging and the motion of the dynamics structures effects in the image. The generation of simulated IVUS images investigate four important aspects: a) The generation, processing and visualization of the data in the format that the doctors use, b) the exploration of some of the artifacts generated by the averaging of the beams, c) the smoothing and treatment of the images to generate sufficient data for the validation of image processing algorithms, and, d) comparison of data generated by the image formation model to the real data. IVUS images can be obtained in a simulated form, from a simple physical model based on the transmission and reception of high frequency sound waves, when these radially penetrate a simulated arterial structure (Fig. 4). We assume for this model that the waves are emitted by a transducer located in the center of the artery, and that these waves propagate radially through the blood and the arterial structures (intima, media and adventitia), being reflected progressively by them. The reflected waves or echoes that return are received by the transducer, that now behaves as a receiver. The time between the emission and the reception of the waves is directly related to the distance between the source and the reflector (Fig. 5). The echo amplitude that is function of the time, is transformed on gray scale and later to penetration depth, so the radial coordinate is determined. If we place a rotatory transducer, make a registry of the corresponding echoes for each angular position of the transducer and combine all the lines obtained from different positions, as a result we will be able to obtain a simulated 2D image of the structure in study. The 3D IVUS simulated can be generated as a sequence of n-planes generated independently, taking into account the arterial deformation caused by the blood pulsatile pressure.

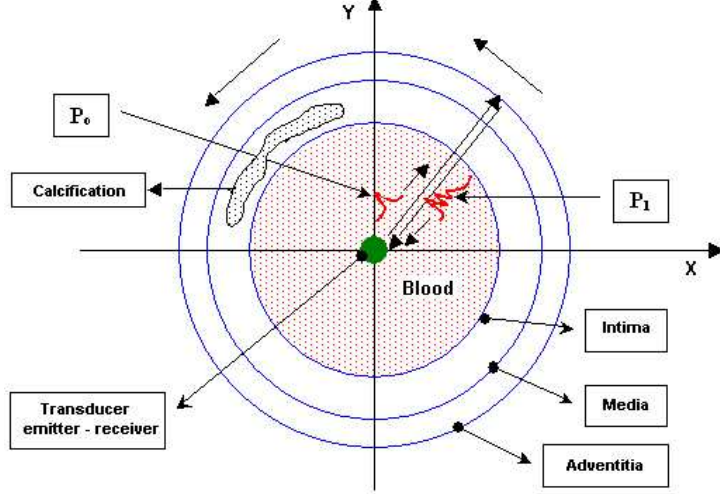


Figure 4: The disposition of the simulated arterial structures (blood, intima, media and adventitia) and calcification are illustrated. The ultrasound rotatory transducer which emits the pulse P_o and receives pulse P_i has been placed at the coordinate center.

0.3 Formal Definition of the Image Model

Let us consider a ultrasound pulse P_o that is emitted at time t_o with speed c from the point with coordinates (r_o, θ_o, z_o) (Fig. 6), and that interacts with the scatterer located at the position, (R, Θ, Z) with the spatial distribution of the differential backscattering cross-section, $\sigma(R, \Theta, Z)$. The reflected pulse P_i for the i -th scatterer is an exact replica [10] of the transmitted sound pulse P_o that will return to the point (r_o, θ_o, z_o) at time $(t_i - t_o)$ and will be out of phase temporarily with respect to the pulse P_o by time difference $\delta = t_i - t_o$ between the emitted pulse at t_i and the received pulse at t_o . The time delay δ is given by:

$$\delta = \frac{2|R|}{c} \quad (1)$$

$$\vec{R} = \vec{r} - \vec{r}_o, \quad \vec{r} = x\hat{i} + y\hat{j} + z\hat{k}, \quad \vec{r}_o = x_o\hat{i} + y_o\hat{j} + z_o\hat{k}$$

We choose a coordinate system (X, Y, Z) with respect to the emitter/receiver position:

$$\vec{X} = (x - x_o)\hat{i}, \quad \vec{Y} = (y - y_o)\hat{j}, \quad \vec{Z} = (z - z_o)\hat{k}$$

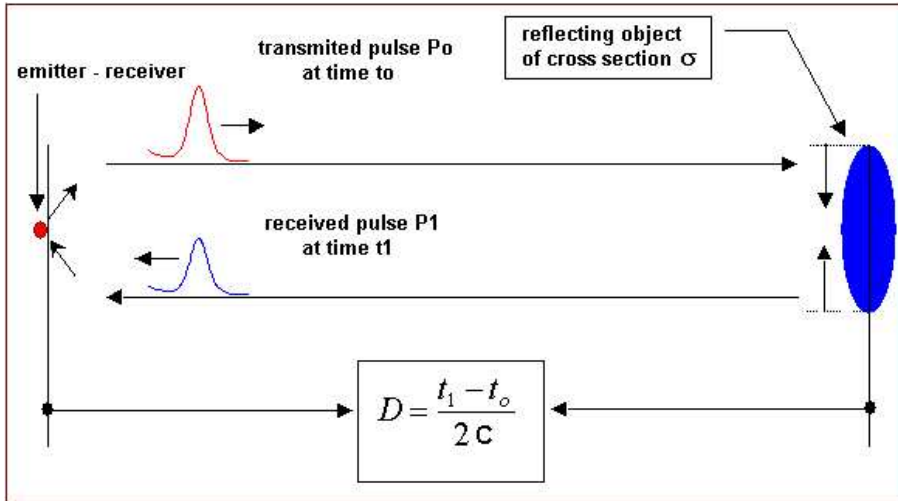


Figure 5: The determination of the distance D between the emitter/receiver and the reflecting object is done from the difference of time between the transmitted pulse P_0 and the received pulse P_1 assuming that the pulse speed c is constant.

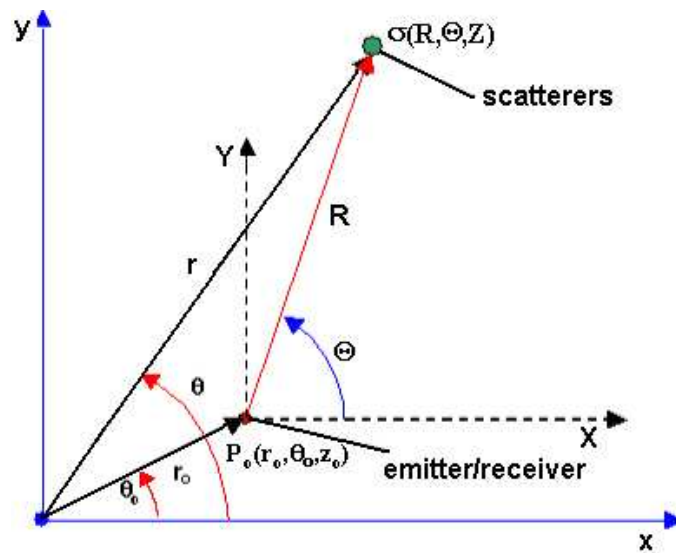


Figure 6: Coordinates system used with the corresponding ultrasound emitter/receiver and the scatterers localization.

and the corresponding cylindrical coordinates given by

$$|R| = \sqrt{X^2 + Y^2 + Z^2}, \Theta = \arctan(Y/X)$$

where $X = |\vec{X}|$, $Y = |\vec{Y}|$ and $Z = |\vec{Z}|$

Assuming the Born approximation [11, 12], the ultrasound reflected signal $S(t, \tau)$ for a finite set of N reflecting scatterers with coordinates (R, Θ, Z) and spatial distribution of the differential backscattering cross-section $\sigma(R, \Theta, Z)$ is given by:

$$S(R, \Theta, Z, t, \tau) = \sum_{i=1}^N \sigma_i(R, \Theta, Z) \zeta_i(t, \tau) \quad (2)$$

where N is the number of scatterers, $\sigma_i(R, \Theta, Z)$ is the spatial distribution of the Differential Backscattering Cross-section (DBC) of the i th scatterer located in position (R, Θ, Z) , $\zeta_i(t, \tau)$ is the transducer impulse function and τ is the delay time which leads to constructive and destructive contributions to the received signal. The Born approximation implies that the scattered echoes are weak compared to the incident signal and it is possible to use the principle of superposition to represent the wave scattered by a collection of particles by adding their respective contribution.

0.3.1 The ultrasound pulse

We consider a planar transducer that is mounted inside an infinite baffle, so that the ultrasound is only radiated in the forward direction. We assumed that the transducer is excited with uniform particle velocity across its face [13, 14]. According to the coordinates system illustrated in the far field circular transducer pressure $P(r, \theta, t)$ (Fig. 8) can be written as:

$$P(r, \theta, t) = j \frac{\rho_o c k a^2 v_o}{2r} \left[\frac{2J_1(ka \sin(\theta))}{ka \sin(\theta)} \right] \exp(j(\omega t - kr))$$

where t is the time, ρ_o is the medium propagation density, c is the sound speed for biological tissue, (typically $c = 1540m/s$), v_o is the radial speed at a point of the transducer surface, a is the transducer radius, \vec{k} is the propagation vector, defined as $k = |\vec{k}| = 2\pi/\lambda$, λ the ultrasound wave length, defined as $\lambda = c/f_o$, f_o ultrasound frequency, $\omega = 2\pi f_o$ and $J_1(x)$ is the first class Bessel function. Fig. 8 shows a graphics of the pressure as a function of ν , where $\nu = ka \sin(\theta)$. In some applications, particularly when discussing biological effects of ultrasound, it is useful to specify the acoustic intensity [16]. The

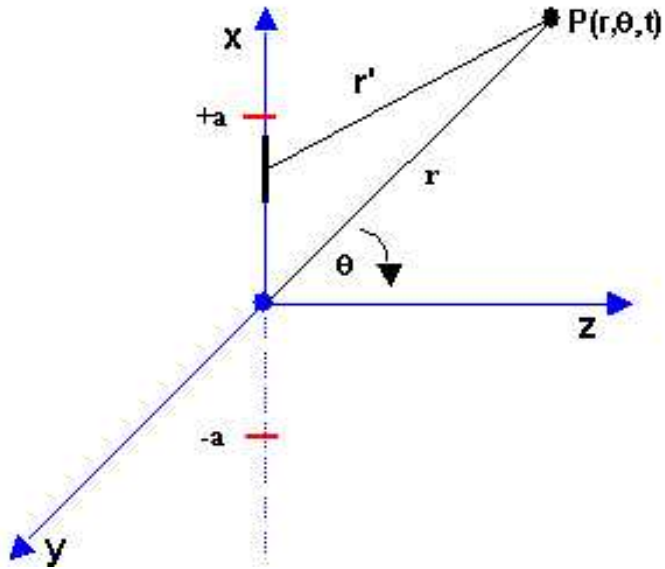


Figure 7: Geometrical variables used for the calculations of the pressure distributions $P(r, \theta, t)$ for a planar circular transducer of radius, a .

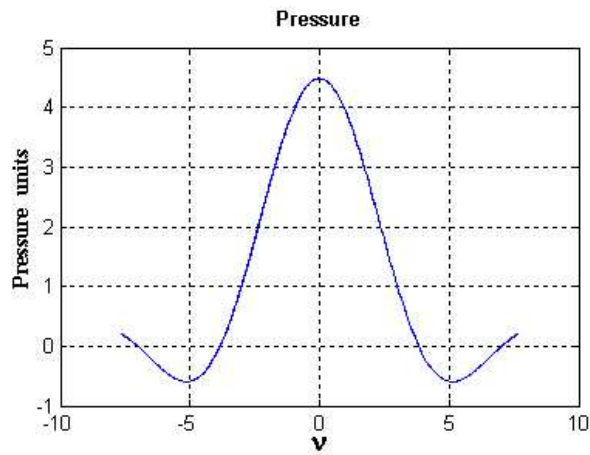


Figure 8: Transducer pressure distribution.

intensity at a location in a ultrasound beam, I is proportional to the square of the pressure amplitude, P . The actual relationship is:

$$I(r, \theta, t) = \frac{P(r, \theta, t)^2}{2\rho c} \quad (3)$$

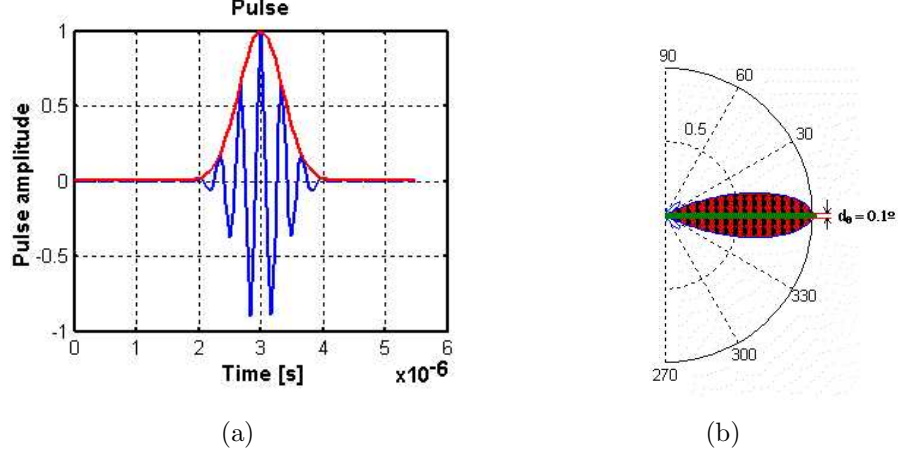


Figure 9: Typical ultrasound pulse and its gaussian envelope (a). The transducer pattern radiation (b).

Again, ρ is the density of the medium and c the speed of the sound. The impulse function $\zeta(t, \delta)$ is generally approximated [15] by a Gaussian (Fig. 9 (a)) which envelopes the intensity distribution and is given by:

$$\zeta(t, \delta) = I(r, \theta, t) \exp\left(-\frac{(t - \delta)^2}{2\sigma^2}\right) \quad (4)$$

where σ is the pulse standard deviation. We consider that the beam is collimated by $\theta = \theta_a$. In our model only the corresponding interval $d\theta \approx 0.1^\circ$ is used that corresponds to the transducer lateral resolution zone (Fig. 9 (b)). Hence Eq. (2) in the transducer coordinate system is based on a discrete representation of the tissue of individual scatterer elements with given position and *DBC* with respect to the transducer coordinates given by:

$$S(R, \Theta, Z, t, \delta) = C_o \sum_{i=1}^N \frac{\sigma_i(R, \Theta, Z)}{|R_i|} \zeta(t, \delta) \quad (5)$$

where δ is given by Eq. (1), $\zeta(t, \delta)$ is the impulse function given by Eq. (4). If we consider only the axial intensity contributions, C_o can be written as[14]:

$$C_o = \frac{\rho_o c k^2 v_o^2 A}{8\pi} \quad (6)$$

where A is the transducer area.

0.4 Principal features of IVUS data.

0.4.1 Image resolution

The resolution is the capacity that has a technique or an instrument to separate in time and/or space two events or objects [14]. At the moment, most of the efforts in the design of new transducers are centered in improving the spatial and the temporal resolution. Unfortunately most of the medical applications demand that the transducers are smaller to increase the resolution but it diminishes their capacity to explore to greater tissues depth. For the IVUS techniques, the resolution plays a very important role since most of the structures to visualize directly depend of these parameters.

0.4.1.1 Axial resolution

The axial resolution is the capacity that the ultrasound technique has to separate the spatial position of two consecutive scatterers through its corresponding echoes [13, 14, 16]. In Fig. 10 a ultrasound pulse P_1 that has a width d_1 frontally affects a linear scatterer array at distance d_{oi} . Each one of the

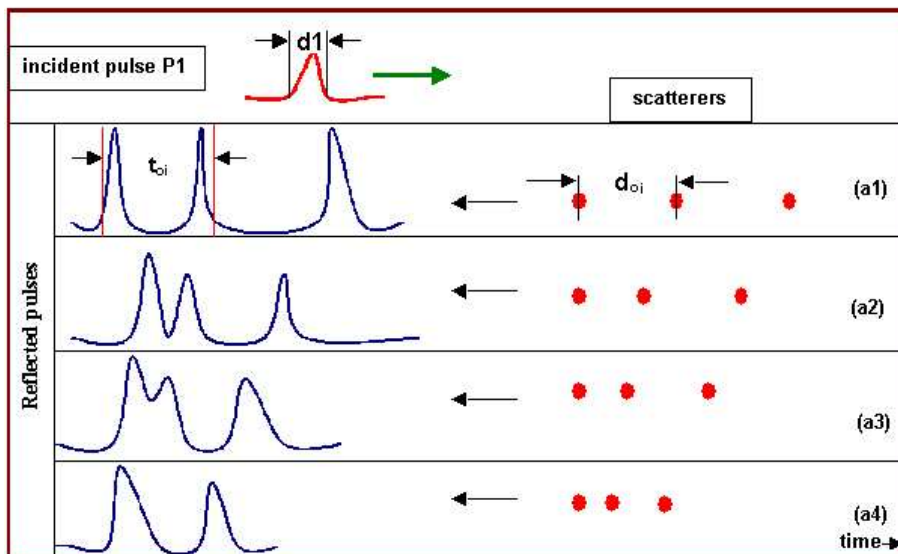


Figure 10: A ultrasound pulse, P_1 that has width, d_1 frontally affects a linear scatterer array placed at distance d_{oi} .

echoes forms a "train" of pulses temporally distanced according to the equation $t_{oi} = 2|R_i|/c$, being R_i the i th relative emitter/scatterer distance and c the pulse propagation speed. The progressive distance reduction of the linear scatterers, given by (a_1, \dots, a_4) (Fig. 10) and (b_1, \dots, b_4) (Fig. 11), reduces the time between the maximums of the "train" pulses. There exists a critical distance width d_t from which the pulses that arrive at the receiver are superposed, not being able, therefore, to discriminate or to separate individually the echoes produced by each scatterer. In Fig. 11 one can observe, that the resolution can be improved by diminishing the pulse width d_t , which is equivalent to increasing the frequency of the emitted pulse. The axial resolution of this

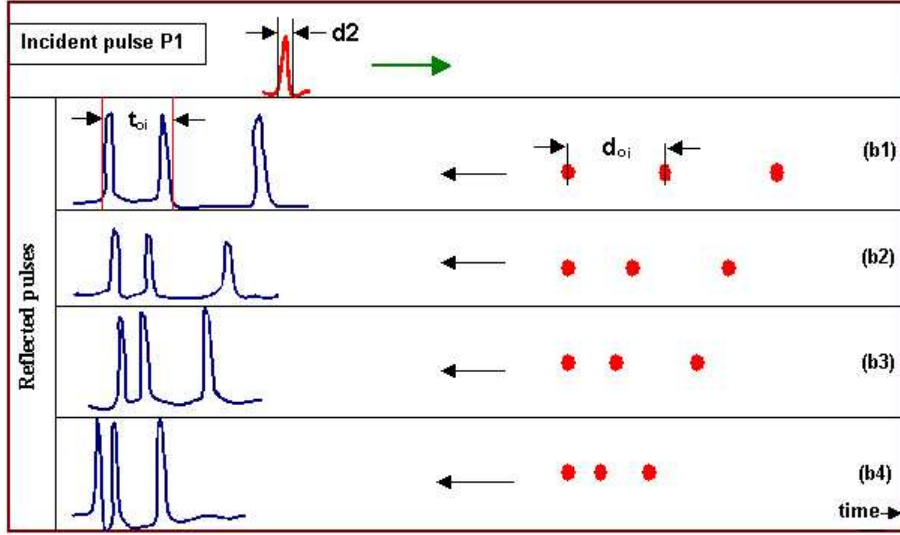


Figure 11: We can see that the progressive distance reduction of the linear scatterers, from (a_1, \dots, a_4) (Fig. 10) to (b_1, \dots, b_4) reduces the time difference between the maximums of the "train" pulses. The maximums can be separated reducing the pulse width from d_1 (Fig. 10) to d_2 , this is equivalent to an increase in the pulse frequency.

technique depends essentially on two factors: **the ultrasound speed** c and **pulse duration** d_t . The functional dependency between the spatial resolution, the frequency and the ultrasound speed propagation is given by:

$$d_r = cd_t = cT = \frac{c}{f} \quad (7)$$

where d_r is the axial resolution, c is the ultrasound speed for biological tissues, d_t is the pulse width, T is the period of ultrasound wave and f is the ultrasound frequency. For the IVUS, the typical values are: $c = 1540$ m/seg and $f = 30$ MHz the axial resolution is approximately: $d_r = 1540/(30 \times 10^6) = 0.05$ mm $\approx 50\mu\text{m}$ and the relative error of the axial resolution is given by:

$$\frac{\Delta d_r}{d_r} = \left| \frac{\Delta c}{c} \right| + \left| \frac{\Delta f}{f} \right|$$

The axial resolution dependency versus the ultrasound frequency is visualized in Fig. 12.

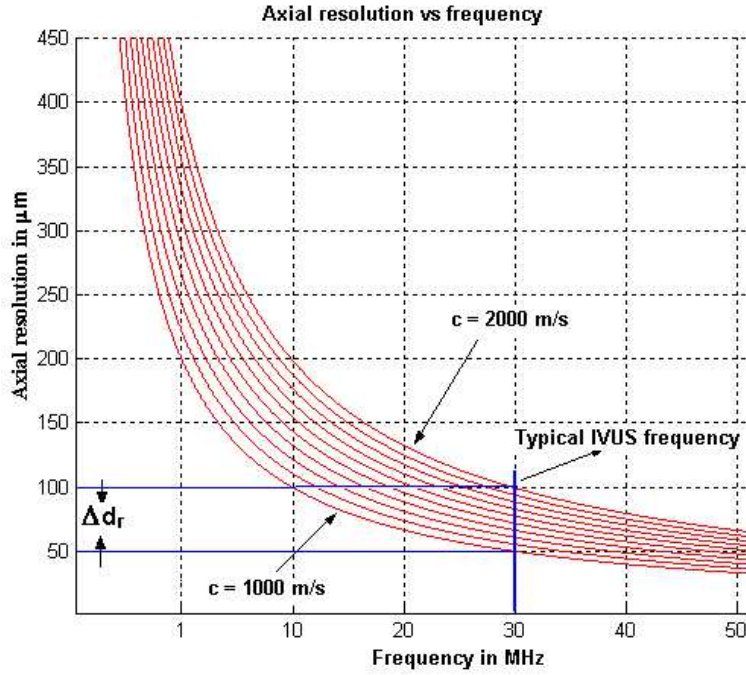


Figure 12: The functional dependency between the axial resolution and the ultrasound frequency for a rank of typical ultrasound speeds in biological tissue. The typical IVUS (30MHz) frequency as well as the tolerance in the axial resolution Δd_r are emphasized.

0.4.1.2 Angular resolution

The angular resolution is the capacity to discern two objects or events located in the tangential direction [13, 14, 16] and depends on the *Beam width*. The

Material	Sound speed (m/s)
Fat	1460
Aqueous humor	1510
Liver	1555
Blood	1560
Kidney	1565
Muscle	1600
Lens of eye	1620
Average	1553

Table 1: Sound speed in selected tissues [16]

beam width depends on the transducer effective emission area (Fig. 13). The

ultrasound transducer lateral resolution d_θ

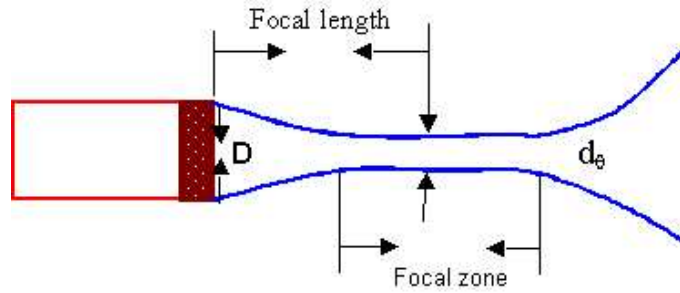


Figure 13: The focal length and the focal zone of a ultrasound transducer are indicated. The transducer lateral resolution d_θ is a function of its diameter, D and the emission frequency, f .

Fig. 14 shows the standard dimensions of typical IVUS ultrasound transducer. The tangential or lateral resolution of a ultrasound emitter of diameter, D that emits by frequency f is given by:

$$d_\theta = 1.22 \frac{\lambda}{D}, \quad d_\theta = 1.22 \frac{c}{D f}$$

and the focal distance (focal length) F is given by:

$$F = \frac{1}{4} \frac{D^2}{\lambda}$$

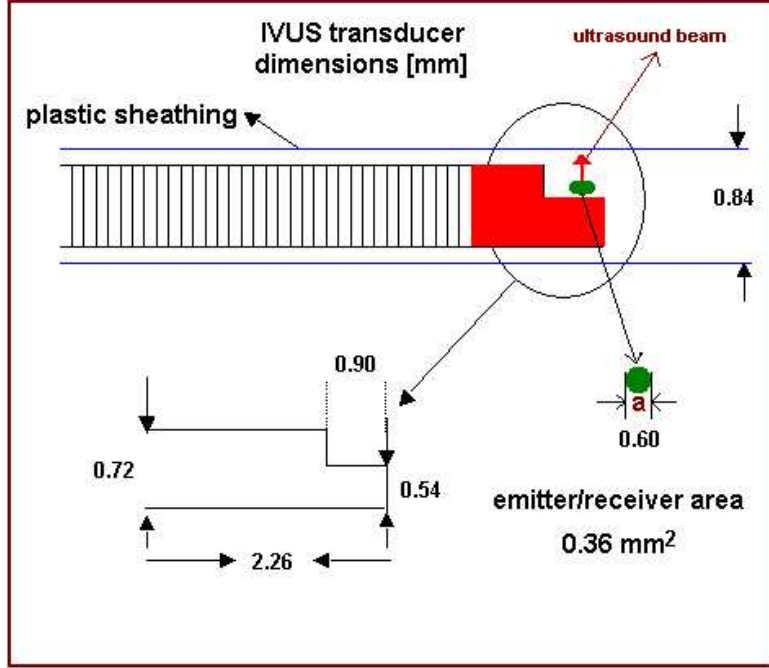


Figure 14: Typical IVUS transducer dimension used by Boston Sci.

where $\lambda = c/f$ and D is the transducer diameter. For a typical transducer of 30 MHz, $c = 1540$ m/seg and transducer dimensions given in Fig. 14, the lateral resolution is $d_\theta \approx 0.10^\circ$ and the focal length is $F = 2$ mm.

0.4.2 The beam intensity

The beam ultrasound intensity, as a function of the penetration depth and the ultrasound frequency, is given by [13, 14, 16]:

$$I(r) = I_o \exp(-\alpha(N_\theta)rf) \quad (8)$$

where I_o is the beam intensity at $r = 0$ and the coefficient, α give the rate of diminution of average power with respect to the distance along a transmission path [17]. It is composed of two parts, one (absorption) proportional to the frequency, the other (scattering) dependent on the ratio of grain, particle size or the scatterer number N_θ located along the ultrasound beam path (See section 0.5.2). Since the attenuation is frequency dependent, a single attenuation coefficient only applies to a single frequency. The attenuation coefficient

of ultrasound is measured in units of dB/cm, which is the log relative energy loss per travelled centimeter. In biological soft tissues, the ultrasound attenuation coefficient is roughly proportional to the ultrasound frequency (for the frequency range used in medical imaging). This means that the attenuation coefficient divided by the frequency (unit $dB/MHz \times cm$) is nearly constant in a given tissue. Typical soft tissue values are 0.5 to 1.0 $dB/MHz \times cm$. In our model we assumed that the attenuation coefficient α is only dependent on the scatterer number in the length way beam. Fig. 15 shows the beam intensity dependence vs penetration depth for several typical frequencies used by IVUS.

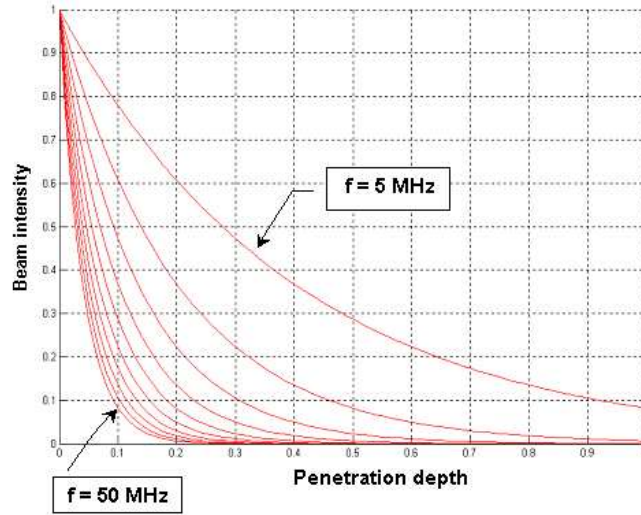


Figure 15: Ultrasound beam intensity versus the penetration depth for several frequencies (5 to 50 MHz).

0.4.3 Ultrasound beam sweeping criterion

Let us explore a criterion that assures that all the return echoes reach the transducer before it moves to the following angular position. Let us define β as the ratio between transducer diameter, D and length arc, ϵ (Fig. 16):

$$\beta = \frac{D}{\epsilon}$$

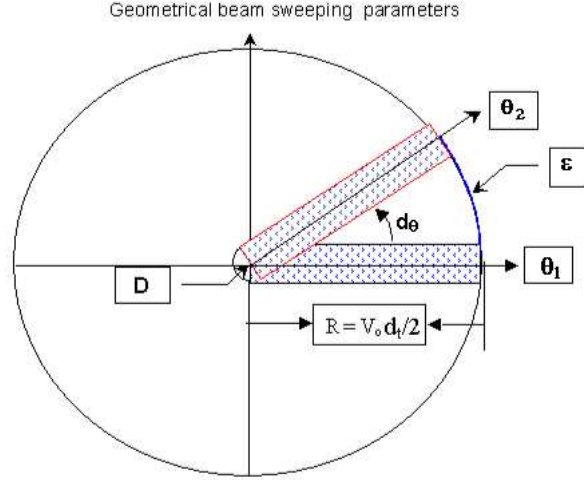


Figure 16: A rotatory transducer emits a radially focused beam. Angular positions, θ_1 and θ_2 define a segment of arc S which can be calculated from the speed of rotation and the speed of propagation of the ultrasound beam.

where D is the transducer diameter and ϵ is the arc segment swept by the beam, between two angular consecutive positions. Note that:

$$d_\theta = \omega d_t, \quad d_t = 2 \frac{R}{c}, \quad \epsilon = R d_\theta \quad (9)$$

Taking into account these definitions, β can be rewritten as:

$$\beta = \left(\frac{r}{R^2} \right) \left(\frac{c}{\omega} \right)$$

where r is the transducer radius, R is the maximum penetration depth, c is the ultrasound speed and ω is the transducer angular speed. The parameter β implies that the transducer area is β times the sweeping area for the rotatory beam and the maximal depth penetration. This assures that a high percentage of echoes incomes to the transducer before it changes to the following angular position. We can determine parameter β by calculating the frequency by which the ultrasound pulse should be emitted. Fig. 17 shows the dependence between parameter β and the transducer angular velocity for several typical velocities in biological tissues. We emphasize the typical IVUS transducer angular velocity. Fig. 18 gives the relation between the sample frequency ($f_m = 1/d_t$) and the typical IVUS transducer angular velocity ω .

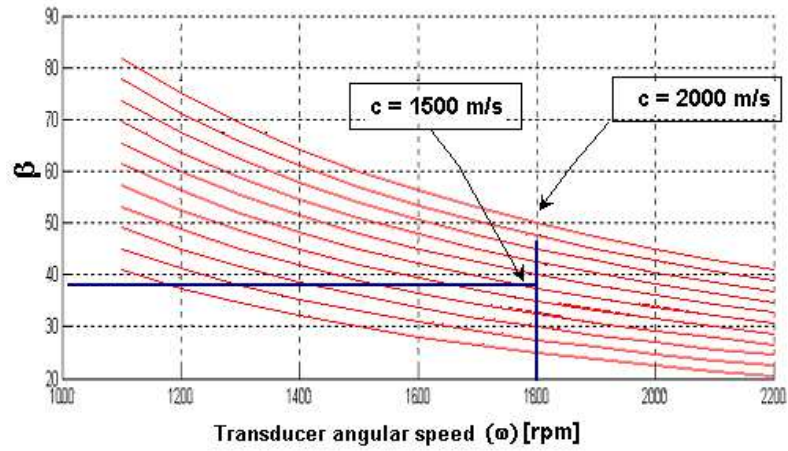


Figure 17: Functional dependence between parameter, β and transducer angular speed, ω

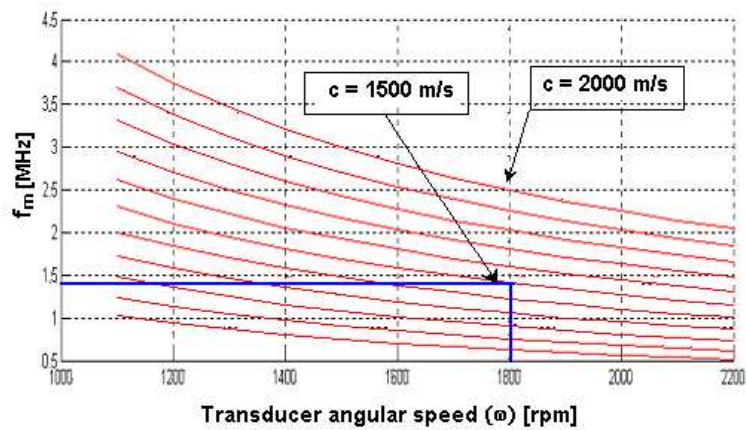


Figure 18: Functional dependence between the sample frequency and the transducer angular speed.

0.4.4 Determining the scatterer number of arterial structures

1) The **Red Blood Cells (RBCs) number** swept by the ultrasound beam (Fig. 19) can be estimated taking into account the plastic sheathing dimen-

sions of the transducer (Fig. 14) and the typical arterial lumen diameter. The

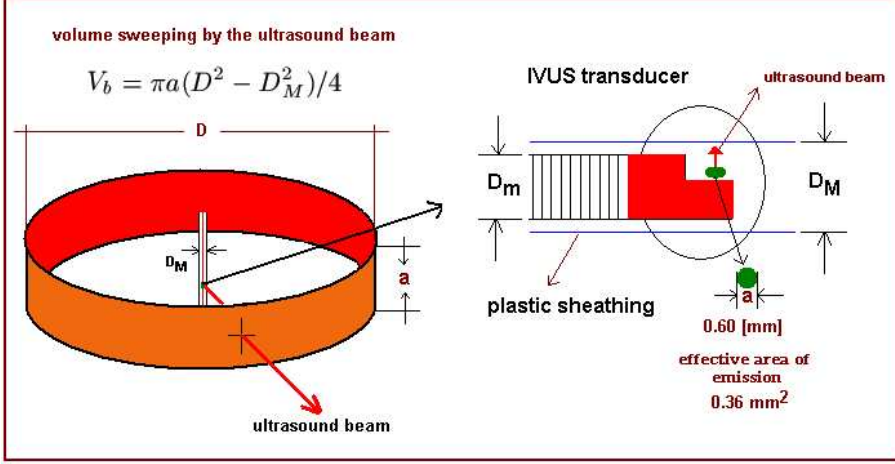


Figure 19: The scatterers volume for each arterial structure can be calculated taken into account the total volume V_b swept by the ultrasound beam.

scatterer number contained in a sweeping beam volume is given by the difference between the sweeping lumen arterial volume, V_a and the plastic sheathing transducer volume, V_t .

$$V_b = V_a - V_t = \pi a(D^2 - D_M^2)/4 \quad (10)$$

where D and D_M are the arterial lumen and the sheathing transducer exterior diameters respectively, and a is the effective emission diameter of the transducer. Typical arterial lumen diameter of coronary arteries is $D \approx 3 \text{ mm}$ [18, 19]. From Fig. 14 we can see that $D_M \approx 0.84 \text{ mm}$ and $a = 0.60 \text{ mm}$. Using Eq. (10) we obtain for the sweeping volume of the transducer beam approximately $V_b \approx 3.91 \text{ mm}^3$. The RBCs can be approximated by spherical scatterers having volume of $87 \mu\text{m}^3$ [20], which corresponds to a radius of $2.75 \mu\text{m}$ (diameter, $d_g = 5.5 \mu\text{m}$). Considering a typical hematocrit concentration [21] of 35% we can estimate the RBCs number by the beam sweeping volume. The RBCs sweeping volume is $V_{rbc} = 1.36 \text{ mm}^3$, and the typical human RBCs number is approximately $N \approx 4.1 \times 10^6 \text{ cells/mm}^3$ [21]. Thus, the RBCs number by the sweeping volume is $N_o \approx 5.61 \times 10^6 \text{ cells}$. The maximal axial resolution at 40 MHz is approximately $d_r = 38 \mu\text{m}$, at this resolution we can observe the

order of $d_r/d_g \approx 7$ RBCs. If we take the scatterers as perfect spheres with radius d_r at maximal axial resolution, we would have of order of 1.37×10^7 scatterers to be simulated. This quantity of RBCs scatterers is not possible to estimate with the actual computer possibilities. In order to generate quantities of scatterer possible to emulate, we generate scatterers groups namely "voxel" [11]. In Table 2, the most important numerical data used by this simulation model are summarized. The minimal structure dimensions able to be

feature	\approx values
Arterial diameter	$D = 3$ [mm]
Sheathing transducer diameter	$D_M = 0.84$ [mm]
Transducer diameter	$a = 0.60$ [mm]
Sweeping volume by the beam	$V_b = 3.91$ [mm^3]
RBC volume	87 [μm^3]
Hematocrit concentration	35 %
RBC volume by 35 % of V_b	1.36 [mm^3]
Typical human RBC number	$N = 4.1 \times 10^6$ [$cells/mm^3$]
Maximal axial resolution at 40 MHz	$d_r = 38$ [μm]
IVUS image resolution	$(1/25) \approx 0.04$ [$mm/pixel$]
Minimal voxel volume	6.4×10^{-5} [mm^3]
Total RBC voxel	360 [voxels]
RBC voxel to be emulated	1.5×10^4 [voxels]

Table 2: Important features and the corresponding approximated values used in this simulation model.

measured by an IVUS image at 40 MHz is $1/25$ [$mm/pixel$] ≈ 0.04 mm. We take this dimension to estimate the minimal "voxel" volume. For the RBCs, $V_o = 0.04 \times 0.04 \times 0.04 \approx 6.4 \times 10^{-5}$ mm^3 . The total number of RBCs per voxel is $N_t = V_o \times N \approx 360$ $cells/voxel$. Now, we can calculate the total RBCs "voxel" number $N_{rbc} = N_o/N_t \approx 1.5 \times 10^4$ $voxels$ for the sweeping volume by the ultrasound beam. This "voxel" number is even computer intractable. Therefore, we must consider that the typical structure dimensions able to be measured by IVUS image are greater than 0.04 mm. A well contrasted image structure by IVUS begins from 0.06 mm. Using these "voxel" dimensions, $V_o = 2.14 \times 10^{-4}$ mm^3 , the total "voxel" number is $N_t \approx 880$ [$cells/voxel$] and

the RBC "voxels" number is approximately $N_1 \approx 6200$ [voxels]. An example of RBCs "voxel" number used in this simulation is given in table 3.

2) **The intima, media and adventitia.** The numerical values necessary for the evaluation of the scatterer number for the intima, media and adventitia were taken from results of L. T. Perelman et. al [22], that give the typical nuclear cells size $l(\mu m)$ distribution for human cells. The "voxel" number for each layer was computed taken into account the typical dimensions of intima, media and adventitia of a normal artery.

3) **The voxel number for the sheathing transducer** was calculated taking into account the minimal scatterers able to be observed at maximal resolution when the frequency is fixed at $40MHz$, a typical IVUS frequency. From Fig. 14 and Fig. 19, the transducer sweeping volume is $V_t = \pi a(D_M^2 - D_m^2)/4$, where, $a \approx 0.60 mm$ is the transducer diameter, $D_M \approx 0.84 mm$ and $D_m \approx 0.72 mm$ are the exterior and interior transducer sheathing diameters respectively. Using these dimensions: $V_t \approx 0.08 mm^3$. The sheathing "voxel" number N_o can be calculated as $N_o = V_t/V_o$, where $V_t \approx 0.08 mm^3$ is the sheathing volume by the beam and $V_o = 4\pi d_r^3/3$ is formed by the minimal spherical scatterers with radius $d_r = c/f$ able to be measured when the frequency f and the ultrasound speed c are known. Taken typical values for $c = 1540 m/s$ and frequency $40 MHz$, $V_o \approx 2.39 \times 10^{-4} mm^3$, thus $N_o \approx 370$ "voxels".

0.5 Simulation of IVUS image

0.5.1 Generation of the simulated arterial structure

Considering the goal of simulating different arterial structures, we can classify them in 3 groups: Tissue structures, non tissue structures and artifacts. The spatial distribution of the scatterer number with a given DBC, $\sigma(R, \Theta, Z)$ at point (R, Θ, Z) has the following contributions:

$$\sigma(R, \Theta, Z) = A(R) + B(R, \Theta, Z) + C(R) \quad (11)$$

where $A(R)$, $B(R, \theta, Z)$ and $C(R)$ are the contributions of tissue structures, non tissue structures and artifacts respectively.

1. **Tissue scatterers.** These are determined by the contribution of the normal artery structures, corresponding to: *lumen, intima, media and*

adventitia. Fig. 20 shows a k -layers spatial distribution of the scatterers for a simulated arterial image. These scatterers are simulated as radial

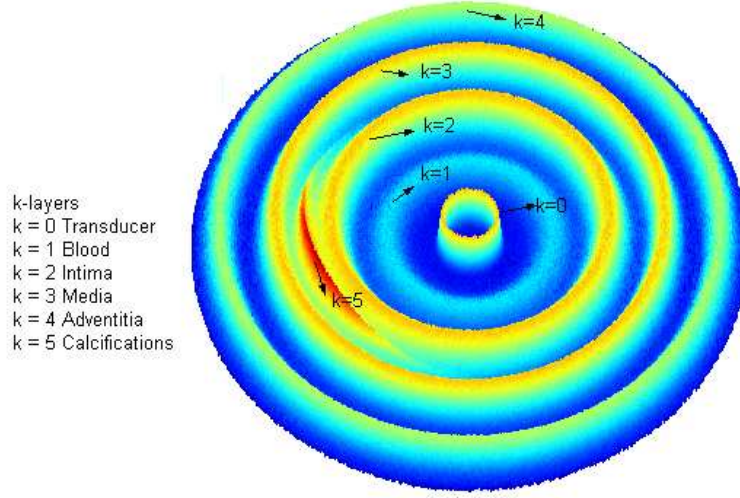


Figure 20: A plane of k -layers simulated artery. The scatterer numbers are represented by the height coordinate in the figure.

gaussian distributions [23] centered in the average radius R_k and having standard deviation η_k corresponding to each arterial structures. Tissue scatterers are represented by:

$$A(R) = \sum_{k=1}^{k_o} \frac{a_k}{\eta_k} \exp\left(-\frac{(R - R_k)^2}{2\eta_k^2}\right) \quad (12)$$

where a_k is the maximal number of scatterers at $R = R_k$, k is the k -th radial simulated tissue layer and R_k is the radial layer average position.

2. **Non tissue scatterers.** These contributions can be originated by structures formed by spatial calcium accumulation, which are characterized because the DBC density is greater than the rest of the arterial structures. They are simulated by a gaussian distribution in the radial, angular and longitudinal arterial position of the simulated structure:

$$B(R, \Theta, Z) = \sum_{l=1}^{l_o} \sum_{m=1}^{m_o} \sum_{n=1}^{n_o} \frac{b_l c_m d_n}{\beta_l \gamma_m \nu_n} F(R, \Theta, Z)$$

$$F(R, \Theta, Z) = \exp \left(-\frac{1}{2} \left(\frac{(R - \bar{R}_l)^2}{\beta_l^2} + \frac{(\Theta - \bar{\Theta}_m)^2}{\gamma_m^2} + \frac{(Z - \bar{Z}_n)^2}{\nu_n^2} \right) \right)$$

where (l, m, n) correspond to the radial, angular and longitudinal axes directions, (l_o, m_o, n_o) are the structures number in radial, angular and longitudinal direction, (b_l, c_m, d_n) are the scatterer numbers that have a maximum at $R = R_l, \Theta = \Theta_m$ and $Z = Z_n$, $(\beta_l, \gamma_m, \nu_n)$ are the radial, angular and longitudinal standard deviation and (R_l, Θ_m, Z_n) are the radial, angular and longitudinal average position.

3. **Artifacts scatterers.** In our model we consider the artefact caused by the sheathing transducer:

$$C(R) = \frac{a_o}{\alpha_o} \exp \left(-\frac{(R - R_o)^2}{2\alpha_o^2} \right)$$

where a_o is the scatterers number that has a maximum at $R = R_o$, α_o is the artifact standard deviation and R_o is the artefact radial average position.

0.5.2 1D echogram generation

To obtain an 1D echogram, a ultrasound pulse is generated by Eq. (4) and it is emitted from the transducer position. The pulse moves axially through scatterers (Fig. 21 (a)), its intensity distribution decreases (Fig. 21 (b)), with the penetration depth and the scatterers numbers on the ultrasound way according to the Eq. (8). The echo amplitude is registered by the transducers (Fig. 22) as a signal function of time $S(t)$ (Eq. 13). The value is transformed to penetration depth replacing $t = x/c$ and normalized to grey scale. The spatial distribution of cross section scatterers, σ is generated by using Eq. (11). Fig. 21 shows the simulations of N scatterers located in $(R_i, \Theta_a \leq \Theta_j \leq \Theta_b)$.

$$S(t, \Theta_o) = \sum_{i=1}^{N_R} \sum_{j=1}^{N_{\Theta_i}} \frac{\sigma(R_i, \Theta_o \pm \Theta_j) \zeta(t, \delta_i)}{|R_i|} \quad (13)$$

$$S(t, \Theta_o) = C_o \sum_{i=1}^{N_R} \sum_{j=1}^{N_{\Theta_i}} \frac{\sigma(R_i, \Theta_o \pm \Theta_j)}{|R_i|} \exp \left(\frac{-(t - \delta_i)^2}{2\sigma^2} \right) \sin(\omega t - \delta_i)$$

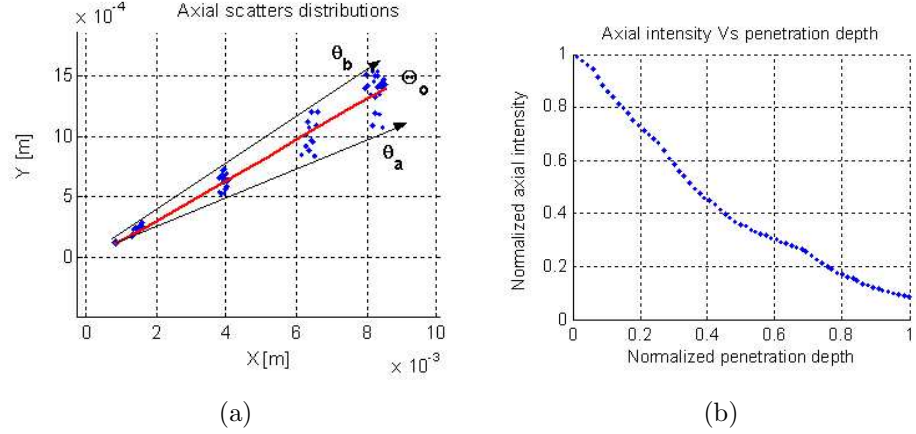


Figure 21: The 1D echogram is obtained by fixing the angular position $\Theta_0 = \bar{\Theta}$ of the ultrasound beam (a). The total signal $S(t)$ is only generated by the scatterers N_{Θ} located in the angular position between $\Theta_a \leq \Theta_0 \leq \Theta_b$. The intensity distribution decreases with the depth penetration and the scatterers numbers N_{Θ} through the beam way (b).

where $\Theta_o = (\Theta_a + \Theta_b)/2$, C_o defines the transducer constant parameters and N_{Θ_i} is the total scatterer number in the angular position between $\theta_a \leq \Theta \leq \theta_b$ for a radial position R_i . The sum only operates on the scatterers located between the angular position $\theta_a \leq \Theta \leq \theta_b$ that is the focal transducer zone (Fig. 9 (b) and Fig. 13). Therefore, N_{Θ} is the total scatterers number in this region. Eq. (13) can be written as a function of the penetration depth, replacing $t = x/c$. Eq. (13) can be rewritten on gray-level scale as:

$$S(t, \Theta_o) = \frac{256}{\max(S(t))} C_o \sum_{i=1}^{N_R} \sum_{j=1}^{N_{\theta_i}} \frac{\sigma(R_i, \Theta_o \pm \Theta_j)}{|R_i|} \exp\left(\frac{-(t - \delta_i)^2}{2\sigma^2}\right) \sin(\omega t - \delta_i) \quad (14)$$

where $\delta_i = 2R_i/c$ and $S(x)$ is the 1D echogram generated by a set of N_{Θ} scatterers located in $(R_i, \Theta_a \leq \Theta_i \leq \Theta_b)$. The overall distribution backscattering cross section, $\sigma_i(R_i, \Theta_i \pm \delta\Theta)$ is given by (Eq. 11).

0.5.3 2D echogram generation

The procedure to obtain the 2D simulated IVUS is the following: A rotatory transducer at angular velocity, ω (Fig. 23 (a)) is located at the center of the

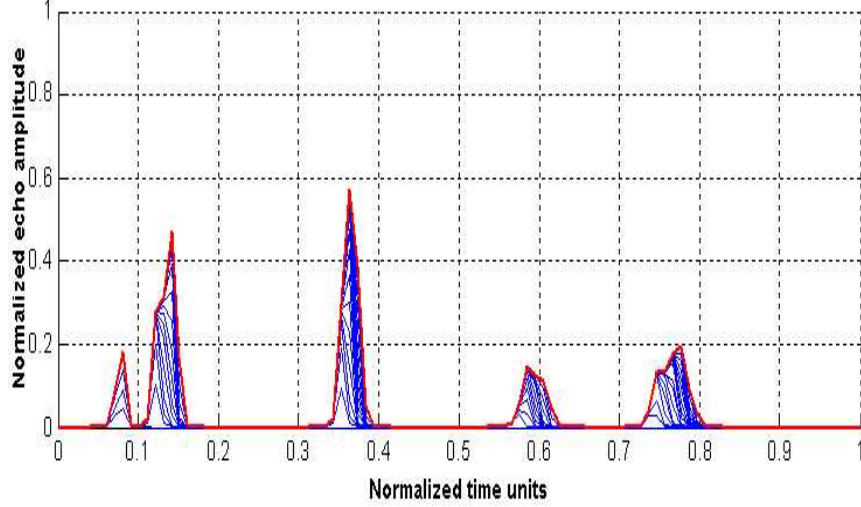


Figure 22: The corresponding echoes are finally transformed to normalized echo amplitude and then to grey level scale vs time or penetration depth.

simulated arterial configuration given by Eq. (11). The transducer emits a ultrasound pulse radially focused at frequency, f_o along angular direction, θ_1 (Fig. 23 (a)). The pulse progressively penetrates each one of the layers of the simulated arterial structure according to Eq. (15). Each one of the layers generates a profile of amplitude or echoes in the time, that can be transformed into a profile of amplitude as a function of the penetration depth (Fig. 23 (b)). Therefore, the depth can be calculated by Eq. (1). As the penetration depth is coincident with the axial beam direction, the radial coordinate, R is thus determined. This procedure is made n -times for the angles, $(\theta_1, \dots, \theta_n)$ and the 2D image is generated. The generated echo profiles are transformed to a polar image, and the intermediate beams are computed (Fig. 23(c)). The image is transformed to cartesian form and the empty pixels are filled (Fig. 23(d)).

Using the ultrasound reflected signal $S(t, \Theta)$ for a finite set of N reflecting scatterer with coordinates (R, Θ, Z) and spatial distribution of the differential backscattering cross-section, $\sigma(R, \Theta, Z)$, the 2D echo signal $S(t, \Theta)$ can be written as:

$$S(t, \Theta) = C_o \sum_{i=1}^{N_R} \sum_{j=1}^{N_{\theta_i}} \frac{\sigma(R_i, \Theta \pm \theta_j) \zeta(t, \delta_i)}{|R_i|} \quad (15)$$

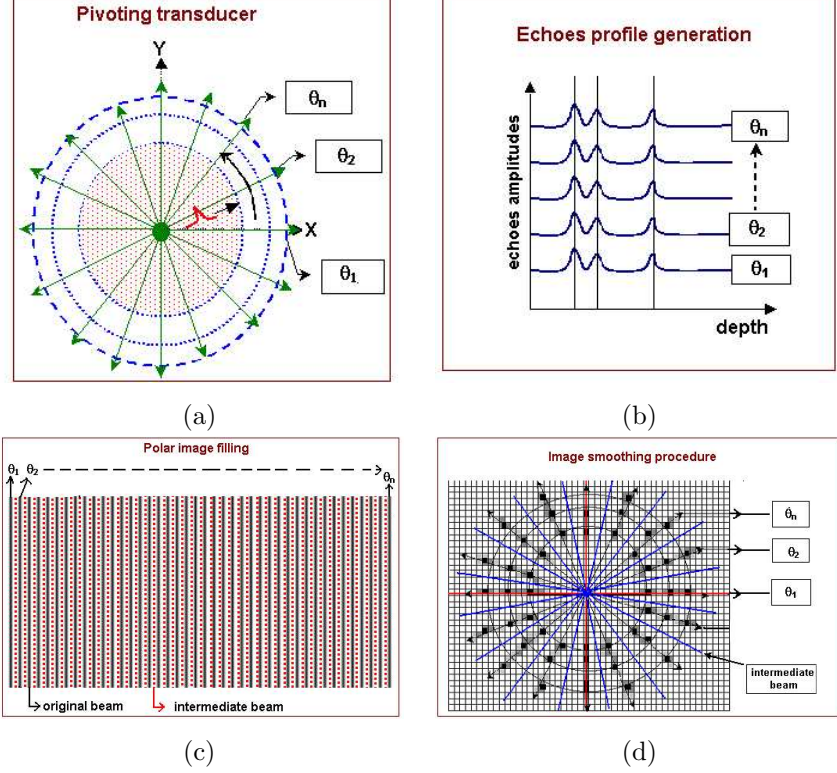


Figure 23: The transducer emits from the artery center (a), echo profile transformed into penetration depth (b), the echo profiles are transformed to a polar image (c), empty pixels filled and the final IVUS image is smoothed (d).

where $S(t, \Theta)$ is the temporally generated signal by a set N_R of scatterer which are localized in angular position θ , $\theta \in [\theta_a, \theta_b]$, N_{θ_i} is the total scatterer number in the angular position between $\theta_a \leq \bar{\Theta} \leq \theta_b$ for a radial position R_i . We consider two forms of $\bar{\Theta}$:

- by no uniform distributed scatterers:

$$\bar{\Theta} = (\theta_a + \theta_b)/2$$

- by uniform distributed scatterers:

$$\bar{\Theta} = \frac{1}{N_R} \sum_{j=1}^{N_R} \Theta_j$$

0.5.4 Final image processing

The actual image obtained only with the original beams is very poor, we must explore several smoothing procedures to improve the image appearance. The procedures to obtain the final simulated image are as follows:

1. The echoes are obtained by the pivoting transducer (Fig. 23 (a)).
2. Each echo profile is ordered according to the angular position (Fig. 23 (b)).
3. The original image is transformed to a polar form (Fig. 23 (c)).
4. Secondary beams are computed between two original neighbor beam (Fig. 23 (c)).
5. The image is smoothed by a 2×2 median filter.
6. The image is again transformed to cartesian form. As result of this transformation a significant number of pixels will be empty (Fig. 23 (d)).
7. The empty pixels are filled in a recursive way form, using for this an average of the eight nearest neighbors (Fig. 23 (d)).
8. An image reference reticle is added and a gaussian filter is applied.

Fig. 24 shows the scatterers distribution for a concentric arterial structure and an axial ultrasound beam position (a), and its corresponding echo profiles (b). Each axial echo is positioned by an angular position (c). In this way, the 2D echogram is constructed (d). The procedure of image smoothing is described in section 0.5.4.

0.6 Validation of the image simulation model

Once defined the generic basic model of IVUS image formation, we need to compare it to real images contrasting the expert opinion to test its use. To this purpose, we defined procedures to extract quantitative parameters that permit to measure the global and local similarity of the images obtained. The main goal of this simulation is to give a general representation of the principal characteristics of the image. The comparison of real and simulated images should

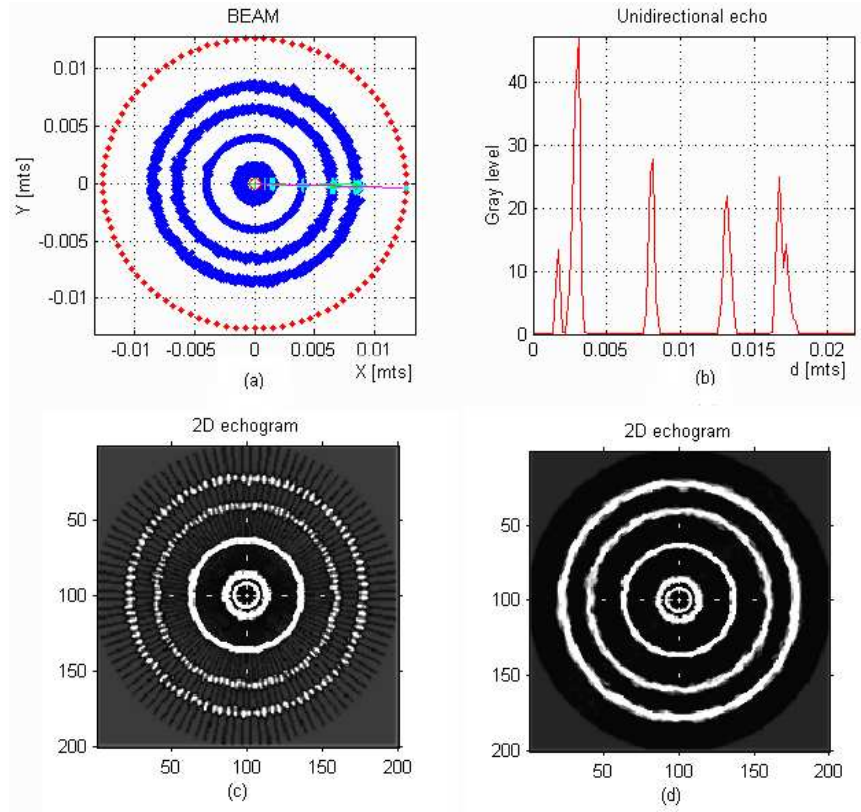


Figure 24: The scatterers distribution (a), the corresponding 1D echoes (b), 2D echogram is constructed (c) and the image is smoothed (d).

be done on the global image descriptors. We concentrated on the distribution of the grey levels. Data such as transducer dimensions (Fig. 14), the catheter as well as the reticle location, operation frequency, band width, original and secondary beam number used for the simulation are standard values used from Boston Sci. [24]. However, the optimal values of frequency and attenuation coefficient are obtained by the cross validation procedure [23]. The dimensions, scatterer number, and the backscattering cross section of the simulated arterial structures were obtained from different literature [7, 10, 11, 19, 22, 24]. Typical values of the RBCs "voxel" numbers took into account the typical hematocrit percentage [11] (section 0.4.4). Instrumental and video noise has been incorporated into the simulated image, due to electronics acquisition data, and the acquisition and processing to the video format.

The zones of greater medical interest (lumen, lumen/intima, intima/media and media/adventitia) were simulated for several real IVUS images. The smoothing image protocol is not known so that the corresponding tests were done until finding the maximal similarity to the real images based on the use of 3 progressive methods. 1) The empty pixels are filled using the average of eight neighbors. 2) A median filter is used, and 3) A gaussian filter is applied in order to find the noise reduction. The quantitative parameters used for the image comparison were directed for global and local image regions, being this:

1. **Grey level average projection**, p_x and p_y , horizontal and vertical image projection, are defined for an $m \times n$ image I as [25]:

$$p_{x(i)} = \frac{1}{m} \sum_{j=1}^m I_{ij}, \quad p_{y(j)} = \frac{1}{n} \sum_{i=1}^n I_{ij} \quad (16)$$

2. We define a global linear **correlation** between real (x) vs simulated (y) data as follows:

$$y = mx + b \quad (17)$$

where m and b are the linear correlation coefficients.

3. **Contrast to Noise Ratio Signal** (CNRS) as figure of merit, defined as [26]:

$$CNRS = \frac{(\mu_1 - \mu_2)^2}{\sqrt{\sigma_1^2 + \sigma_2^2}} \quad (18)$$

where μ_1 , μ_2 , σ_1 and σ_2 are the mean and the standard deviation inside the regions of interest (ROIs).

0.6.1 Scatterer radial distribution

The radial scatterer distribution is an important factor for a good image simulation. The scatterers under consideration in this simulation are: the transducer sheath, blood, intima, media and adventitia. We can obtain the arterial structure configuration from an emulated form and from a real validated IVUS image. For the study of the synthetic images we have used two procedures:

1. **Standard data.** Typical geometric arterial parameters and its interfaces: lumen/intima, intima/media and media/adventitia are obtained from standard literature.

2. **Validated data.** Geometrical parameters are obtained from a manually segmented IVUS images.

In order to investigate the image dependencies of IVUS parameters (frequency, attenuation coefficient, original beam number, secondary beam and smoothing procedures), we have used a standard data procedure, using for this modality a concentric scatterer distribution. To compare simulated images to real data, we use manually segmented real images, that correspond to the validated data procedure. In a manually delineated structures of IVUS images, we extract the position radius R_k of lumen, intima, media adventitia and transducer sheath. Figure 25 shows typical 2D spatial scatterer distributions obtained from standard procedure for the most important arterial structures and the scatterer artefact caused by the transducer sheath.

The radial scatterer distributions play a crucial role in the definition of the IVUS images because they define the ultrasound attenuation in the axial direction. Medical doctors have special interest in grey level transition in the interface of two media. For instance, the lumen/intima transition defines the frontiers of the lumen. These transitions can only be found through a good radial scatterer distribution.

The radial scatterers distribution of the typical arterial structures and the transducer sheath are shown in Fig. 26.

0.6.2 DBC distribution

The k-layers DBC_k values for a typical simulated arterial structure are shown in Fig. 27 and Fig. 28. There the count of scatterers of each tissue is shown as a function of the cross section of scatterers. The numerical values are given in Table 3 [27].

0.6.3 IVUS image features

0.6.3.1 Spatial Resolution

A good spatial resolution gives the possibility of improving the visualization of the lumen/intima transition and studying the structures that means an important information for medical doctors. Typical numerical parameters such as: *Scatterer number* N_k , k-layer average radial position \bar{R}_k , its standard deviation η_k , the DBC k-layer mean μ_k , and its standard deviation σ_k are given in Table

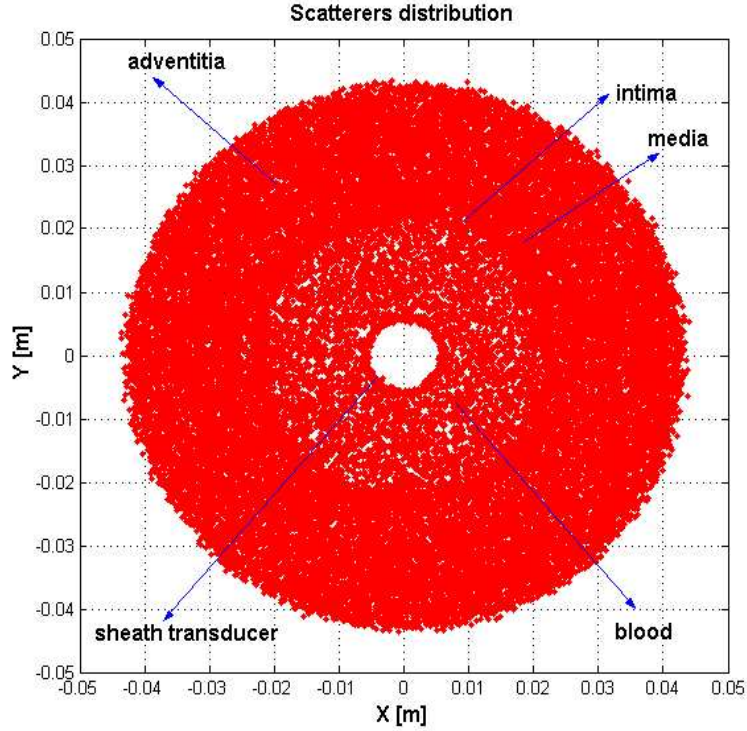


Figure 25: Typical concentric 2D scatterer distribution for the most important simulated arterial structures (blood, intima, media, and adventitia) and the scatterer artefact generated by the transducer sheath.

3. The typical IVUS parameters used in this simulation are given in Table 4. The typical cell nuclear size was obtained by Perelman et al [22]. In Fig. 29 we can observe the dependency of axial resolution and the ultrasound frequency. To illustrate this, four IVUS simulated images are shown. *Low frequency* ranging from 10 to 20 MHz correspond to an axial resolution from 154 to 77 μm , *intermediate frequency* from 20 to 30 MHz gives axial resolution from 77 to 51 μm . In these cases, it is possible to visualize accumulations around 100 RBCs *High frequency* from 30 to 50 MHz lead to 51 to 31 μm of axial resolution. Moreover, it is now possible to visualize accumulations of tens RBC's. The IVUS appearance improves when the frequency increases, allowing that different structures and tissue transition interfaces are better detected.

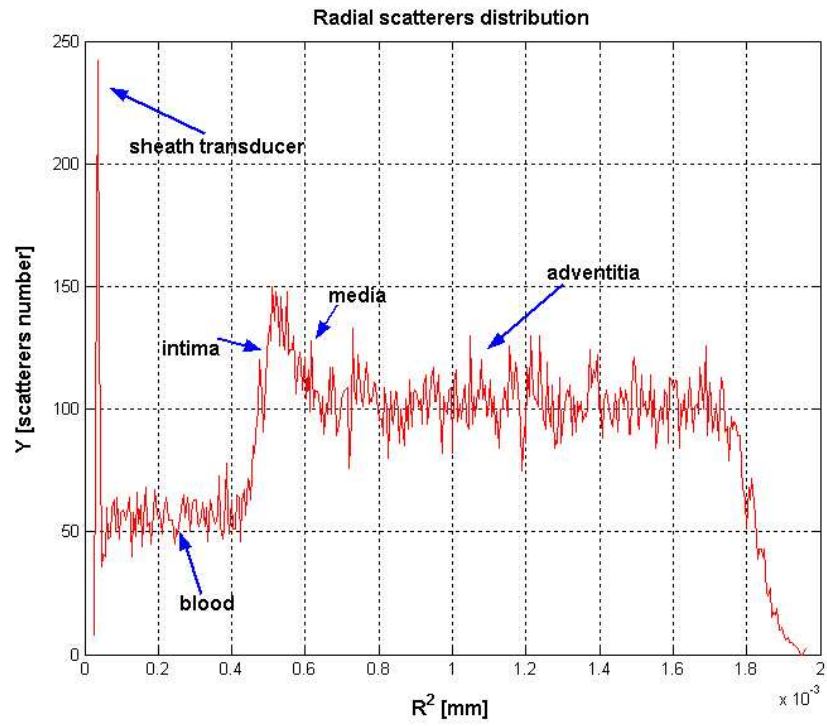


Figure 26: Radial scatterer distribution for the arterial structure: blood, intima, media, adventitia, and the transducer sheath.

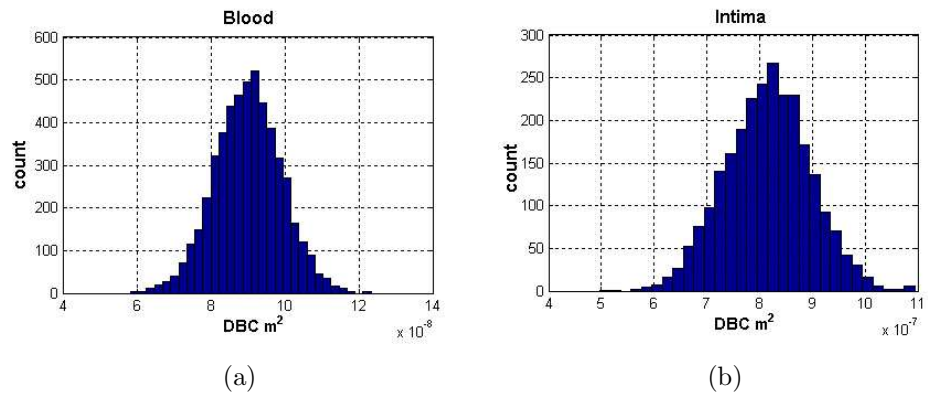


Figure 27: DBC distributions of simulated arterial structures, blood (a) and intima (b).

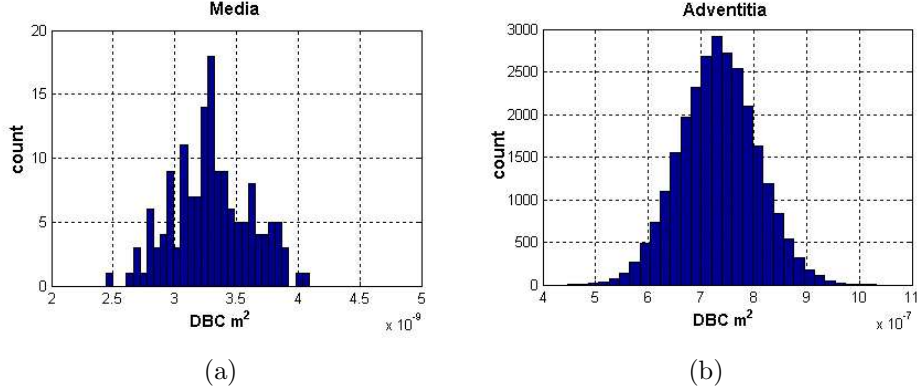


Figure 28: DBC distributions of simulated arterial structures, media (a) and adventitia (b)

0.6.3.2 Optimal Ultrasound Frequency

In order to validate our model, we compare synthetic to real images. We generated synthetic images for a great rank of frequency and used cross validation method [23] to find out the most similar image to the real one generated by Boston Sci. equipment at 40 MHz of frequency. The sum square error (SSE) from the real to the simulated images for each ultrasound simulated frequency is computed. Fig. 30 (a) shows the SSE versus ultrasound frequency. The optimal frequency is located in the interval of 40 to 50 MHz. Note that the central frequency of Boston Sci. equipment is 40 MHz, therefore it can be considered as an evidence to show the correctness of the method.

0.6.3.3 Optimal Attenuation Coefficient

We have emulated synthetic IVUS images with different attenuation coefficients, the optimal attenuation coefficient was tested by applying the cross validation method of the synthetic images vs the real images. Fig. 30 (b) shows SSE vs attenuation coefficient α , the optimal attenuation coefficient obtained was $0.8 \text{ dB}/[\text{MHz cm}]$. There is a range of suboptimal attenuation coefficient values for a fixed ultrasound frequency; it is due to the great axial variability of scatterers. However, the attenuation coefficient can be taken as constant for each simulated region [28], although in the transition zones (lumen/intima, intima/media and media/adventitia) the attenuation gives great variability. For this reason, we must average the attenuation coefficient value.

k	structure	N_k	\bar{R}_k [mm]	η_k [mm]	$(DBC)\mu_k$ [m ²] $\times e - 6$	σ_k [m ²] $\times e - 6$
0	Transducer	475	0.59	0.05	7.2e-1	2.68e-2
1	Blood	6204	1.57	1.22	9.0e-2	9.48e-1
2	Intima	729	2.18	0.25	8.2e-1	2.86e-2
3	Media	150	2.38	0.35	3.3e-3	1.82e-1
4	Adventitia	25794	3.44	3.02	7.3e-1	2.71e-2

Table 3: An example of simulated values of arterial structures: N_k is the scatterer number, \bar{R}_k is the mean radial position, η_k is the radial deviation, μ_k is the backscattering cross section and σ_k is the DBC deviation.

It is very important to find out that the optimal frequency is approximating the standard central ultrasound frequency 40 MHz and that the attenuation coefficient is near to the standard values of biological tissues being this from 0.5 to 1 [dB/MHz cm]. This result can be used in different ways: First, to check the used simulation parameters in the case of ultrasound frequency, and second to find structures of interest when the attenuation coefficient is known.

0.6.3.4 The beam number influence

Fig. 31 shows the appearance of several simulated IVUS images when the original and intermediate beam numbers are changed. We obtained the best appearance when the original beam number was 80 and the secondary beam was 240. In total, 320 beams were used by the simulation. We can see that the IVUS appearance in the tangential direction is affected significantly by the beam number change. The total beams for the standard IVUS equipment is normally between 240 to 360 beams [24].

0.6.4 Real vs simulated IVUS

In order to compare the real and simulated IVUS images, we have generated 20 synthetic images with morphological structures corresponding to the structures of a set of real images. We have used a real IVUS image with manually delimit-

parameter	magnitude
Ultrasound sound speed	1540 m/s
Maximal penetration depth	$2e - 2$ m
Transducer angular velocity	1800 rpm
Transducer emission radius	$3e - 4$ m
Attenuation coefficient α	0.8 dB/[MHz cm]
Ultrasound frequency	10 to 50 [MHz]
Beam scan number	160 to 400
Video noise	8 [gray level]
Instrumental noise	12.8 [gray level]
beta parameter	$\beta=38.5$ [ad]

Table 4: Typical IVUS simulation magnitudes

ited lumen, intima, and adventitia to obtain the average radius location, \bar{R}_k for each arterial structure. We applied the optimal frequency of 46 MHz and attenuation coefficient 0.8 [dB/MHZ cm]. Figure 32 (a) shows an IVUS real image of right coronary artery, obtained by a 40 MHz Boston Sci. equipment. Fig. 32 (b) shows a simulated image obtained at the optimal ultrasound simulation frequency 46 MHz. In the real image, we can observe a guide zone artifact (12 to 1 o'clock) due to the guide presence; this artifact will not be simulated at this study. The horizontal ECG base line appears as an image artefact on the bottom of the real image. The global appearance of each image region (lumen, intima, media and adventitia) and their corresponding interface transitions (lumen/intima, intima/media and media/adventitia) are visually well contrasted, compared to the real image. A good quantitative global measure for comparison is the average grey level projection that allows a simple form to find the main image correlated characteristics in an 1D shape grey level profile. Gray level base line, video noise, instrumental noise, reticle influence and the main grey level distribution incoming from the main arterial structures are roughly visible from the grey level average projection. The average grey level projection gives a global measure of similarity between real and simulated images. The similarity measured can be computed for example by the local attenuation coefficient of the projection profile of each ROI [28]. Fig. 33 gives the projections in the horizontal and vertical direction for the real (Fig. 32(a)) and simulated (Fig. 32(b)) IVUS images. The correlation coefficients, m and b (Fig. 34) for

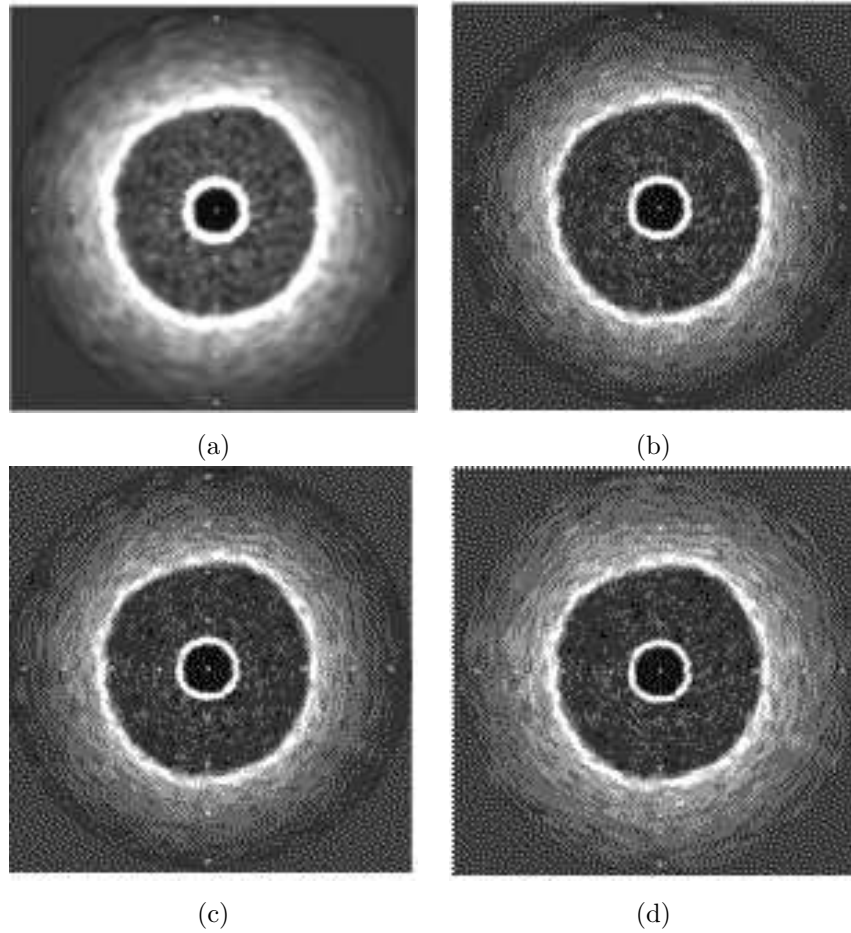


Figure 29: Synthetic images generated by low frequency: 10 MHz (a) and 20 MHz (b), intermediate frequency of 30 MHz (c) and high frequency of 50 MHz (d).

the gray level average projection in the horizontal ($m = 0.63, b = 13.53$) and vertical ($m = 0.75, b = 9.07$) directions, show a positive correlation between the real and simulated data. Fig. 35 shows two selected regions of interest, of the real (Fig. 32 (a)) and simulated (Fig. 32 (b)) image. We can see a good gray level distribution and a soft grey level decay from the center to the peripheries of the IVUS image, produced by the inverse relation between the ultrasound intensity and the penetration depth. The other reason is that the normal attenuation is caused by the scattering intensity given by the tissue

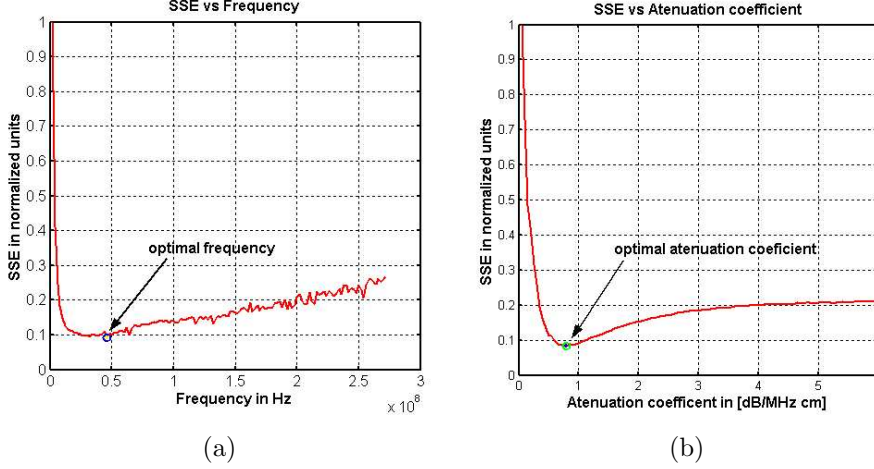


Figure 30: The optimal ultrasound simulation frequency $f_o \approx 46MHz$ (a) and the optimal attenuation coefficient (b) $\alpha \approx 0.8dB/(MHz\ cm)$ are obtained by the cross validation method.

impedance. The Fig. 36 show grey level average profiles in vertical direction Fig. 36 (a) and (c) and horizontal direction Fig. 36 (b) and (d) of the selected ROIs from Fig. 32 (a) and (b). The linear correlation coefficients, m and b (Fig. 37) for the grey level average projection in the horizontal direction ($m = 0.87, b = 4.91$) and vertical direction ($m = 0.85, b = 5.79$), show a significant grey level correspondence between the real and simulated ROIs image.

0.6.5 Polar images

A polar representation of IVUS images offer several advantages: 1) The ROIs to study are very easy to be selected. 2) We can compare the artifact generated by the smoothing procedures. 3) Radial and angular comparison are totally separated, therefore the transition zones in each directions are very easy to be observed. Fig. 38 shows a real (a) and simulated (c) cartesian IVUS images and the corresponding real (b) and simulated (d) polar transformations. A ROI was selected from the real and simulated polar images and the correlation coefficients were obtained. Figure 39 (a) shows the grey level average vertical projection for the real and simulated ROIs data (delineated in red in Fig. 38).

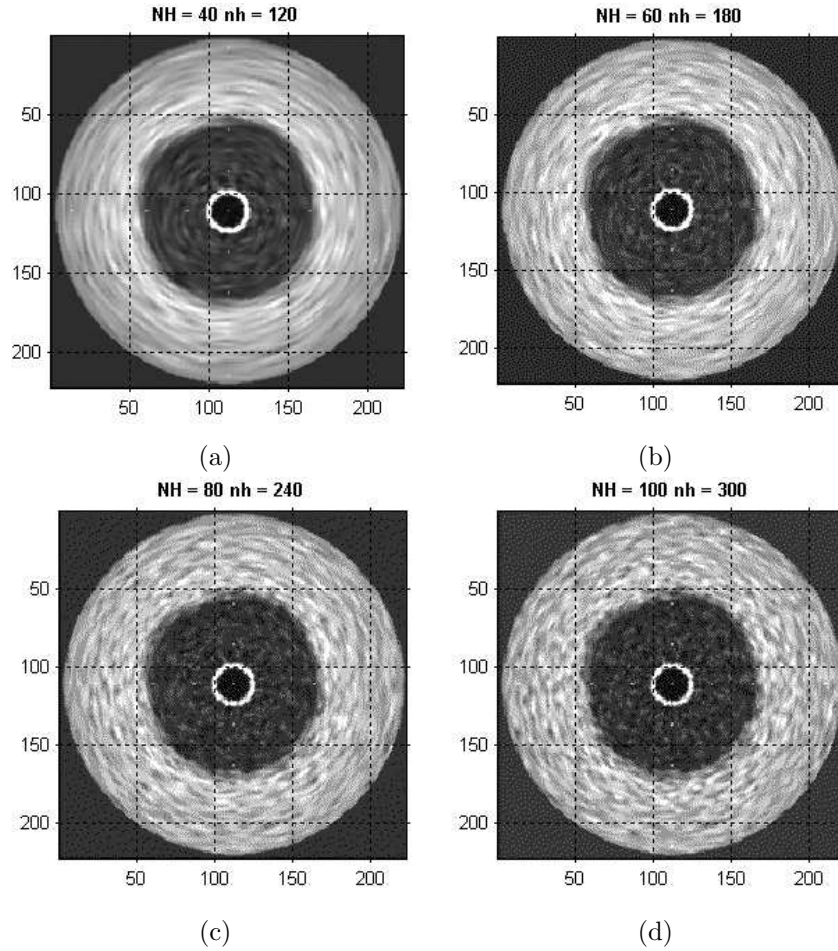


Figure 31: Different combinations of original (NH) and intermediate (nh) beams yield different IVUS appearance.

We can see that the grey level profile of the transition of arterial structure in the lumen/intima, intima/media and media/adventitia are very well simulated, being the linear correlation coefficients $m = 0.93$ and $b = 1.61$ (Fig. 39 (b)). The *global horizontal profile* of the polar images along the projection θ (Fig. 40 (a) and (b)) gives a very important and comparative information about the real and simulated gray level average of arterial structures. The information that can be extracted is relative to the global gray level distribution. The histogram (Fig. 40 (b)) of grey level differences between the horizontal profile of real and simulated data, indicates a very good correspondence (mean $\mu = 8.5$

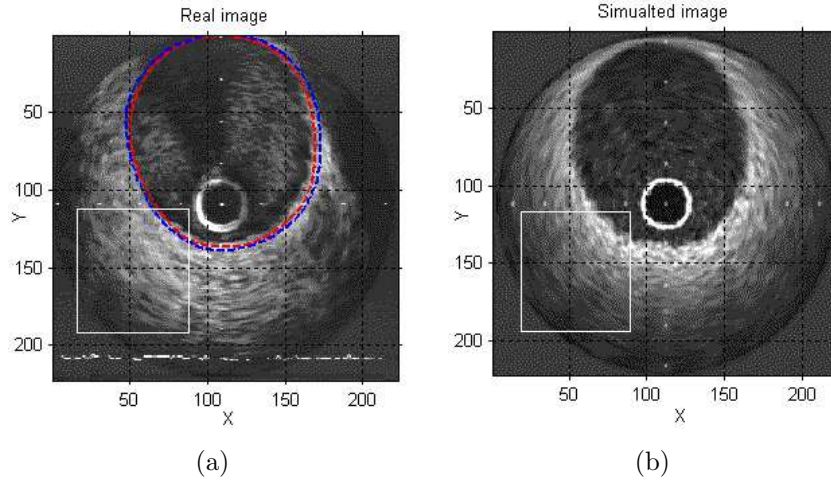


Figure 32: Real (a) and simulated (b) IVUS images segmentation. ROIs are given as squares. Manual segmentation of the vessel is given in (a).

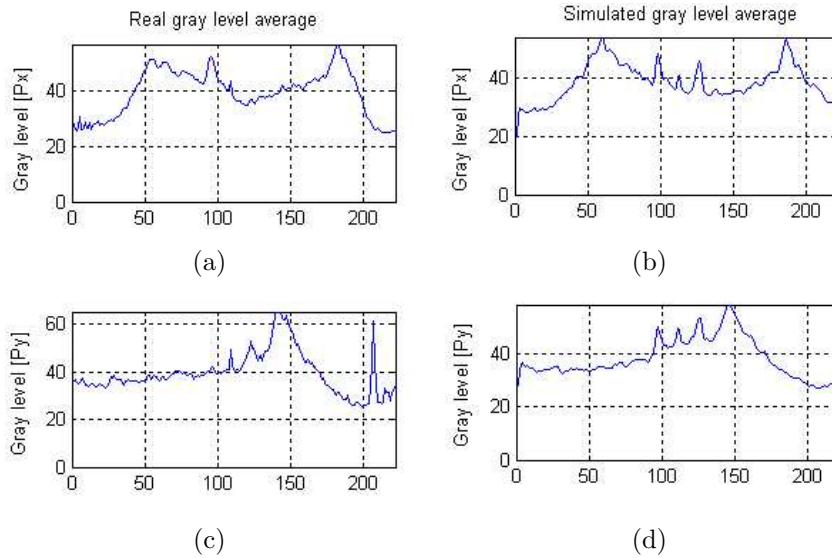


Figure 33: Horizontal (a) and (b) and vertical direction (c) and (d) gray level profile average projections, from real (Fig. 32 (a)) and simulated (Fig. 32 (b)) IVUS images.

and deviation $\sigma = 10.2$). Fig. 41 (a) shows the global projection in the radial direction (the vertical profile). We can see a very good correspondence between

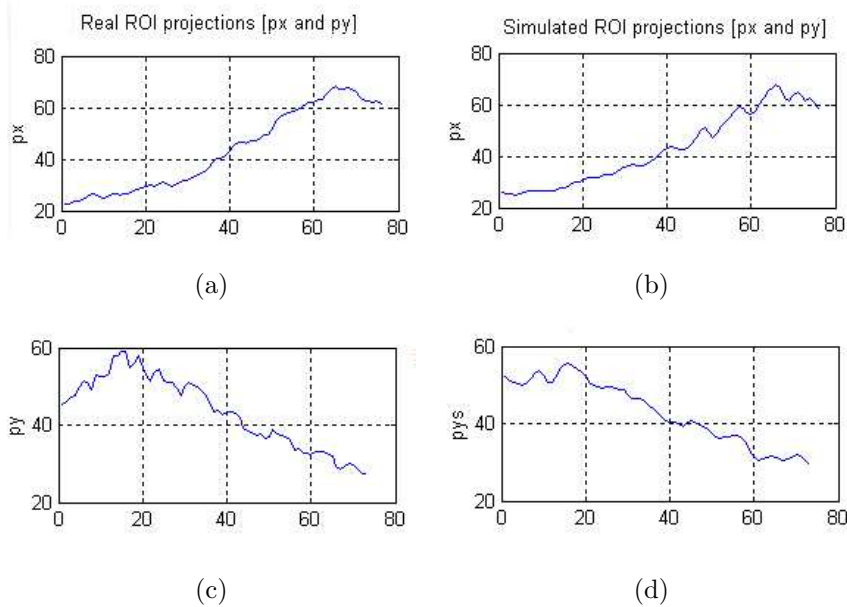


Figure 36: Horizontal (a) and (b) and vertical (c) and (d) projections of (Fig. 35(a)) and simulated (Fig. 35(b)) ROIs IVUS images.

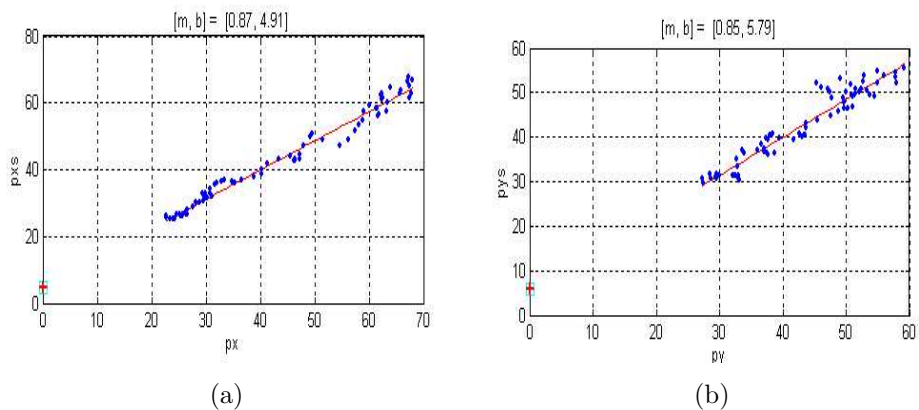


Figure 37: Grey level average correlation, horizontal projection simulated (pxs) vs real(px), obtained from Fig. 36 (a) vs (b) and vertical simulated (pys) vs real (py) data, from Fig. 36 (c) vs (d).

The maximal difference profiles are localized in the transducer sheath gray level distribution, and the base line of the transducer sheath inner region. These differences can be smaller increasing the video and instrumental noise. The high

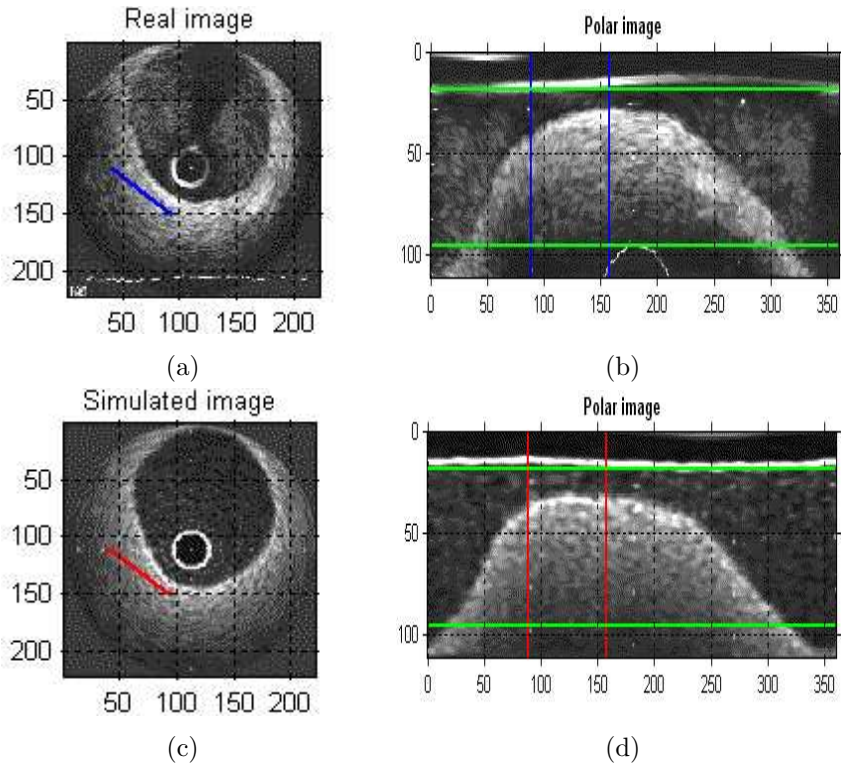


Figure 38: Real (a) and simulated (c) cartesian images and their corresponding real (b) and simulated (d) polar transformation.

frequency oscillations in the gray level profiles come from the concentric arterial structures. We can also observe the gradual reduction of the gray level magnitude from intima/media interface to adventitia, caused by the ultrasound intensity attenuation.

Next step of the validation of the model is to show the significant correspondence between real and simulated gray level distribution data in the medical zones of interest. To this purpose, 20 validated real IVUS images and their corresponding ROIs were selected. The spatial boundaries of the morphological structures of the real data are kept in the synthetic data. Fig. 42 (a) shows 10 real and their corresponding simulated (b) synthetic images. The polar images are shown in figure 43.

Figure 44 shows the simulated vs real gray level correlation for the polar ROI's images selected as shown in Fig. 38. The linear correlation coefficients show a good gray levels correspondence, being these $m=0.90$ and $b=1.42$. The best correspondence is located by low gray levels (20 to 40 gray levels), lumen scatterers, lumen/intima transition, and adventitia. The transition of intima/media and media/adventitia (45 to 60 gray levels) indicate a gradual dispersion. The CNRS average presents a significative uniformity values, $\mu = 6.89$ and $\sigma = 2.88$, for all validated frames. The contrast to noise ratio CNRS as figure of merit for each arterial validated region is shown in Fig 45. The CNRS region mean, standard deviation, and the SSE values referring to the 20 image frames are summarized in table 5. The lumen is a good simulated region, mean,

<i>ROI</i>	<i>mean</i>	<i>std</i>	<i>SSE</i>
Lumen	0.46	0.42	47.68
Intima	10.0	4.38	12.63
Media	9.91	5.14	15.05
Adventitia	7.21	2.76	4.28

Table 5: CNRS mean, standard deviation (std) and sum square error for different tissues structures.

$\mu = 0.46$ and deviation $\sigma = 0.42$. The explanation is that the lumen is not a transition zone, the attenuation ultrasound intensity in this region is very poor (1 to 2%), which determines a simple grey level profile.

The histogram grey level differences for each region of interest in the 20 validated frames are displayed in Fig. 46 and Fig. 47. Table 6 explains the distribution center, μ and the standard deviation, σ for the grey level difference distribution for each simulated region. The minus sign in the mean values

<i>ROI</i>	μ	σ
Blood	-2.44	15.13
Intima	-18.56	24.01
Media	-17.82	22.62
Adventitia	-13.30	14.27

Table 6: Mean and deviation of the ROIs gray level differences referred to histogram from Fig. 46 and Fig. 47.

means that the simulated images are brighter than the real images. A symmetric Gaussian can be seen in the lumen gray level differences distribution, with mean $\mu = -2.44$ and deviation $\sigma = 15.13$. The intima distribution has a mean of $\mu = -18.56$ and deviation of $\sigma = 24.01$, and the media region has a mean of $\mu = -17.82$, and a deviation of $\sigma = 22.62$. The grey level differences distribution displays a light asymmetry. As a result, the simulated image tends to be brighter than the real image. The adventitia gray level differences values show a symmetric distribution with a center of $\mu = -13.30$, and a deviation of $\sigma = 14.27$.

It is very important to note that the gray level difference distribution exhibited Gaussian distributions for all regions of interest. Certainly, the synthetic image brightness is an open problem of the image formation model. A simplest approach is to vary it by modifying the original intensity I_o of the ultrasound beam, similar to the offset of the image acquisition system. Real and simulated gray level distributions for each region of interest are shown in Fig. 48 and Fig. 49. We can note the great similarity in the grey level distributions profile. Figure 50 shows the grey level histogram of the different tissues structures that appear in IVUS images. As expected, it can be seen that the grey level the distributions of different structures overlap and as a result it is not possible to separate the main regions of interest in IVUS images, using only the gray level distributions as image descriptors.

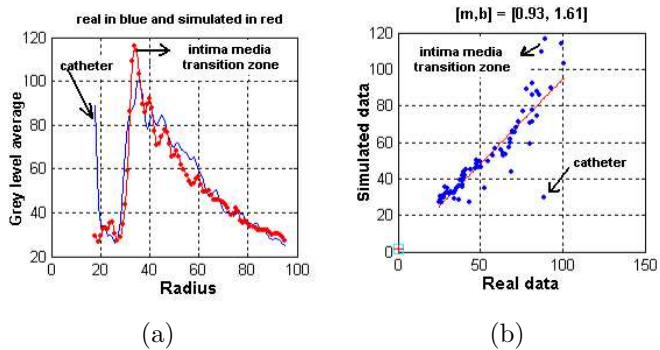


Figure 39: Real(in blue) and simulated (in red) grey level vertical profile (a) of ROIs of Fig. 38 (b) and data correlation (b).

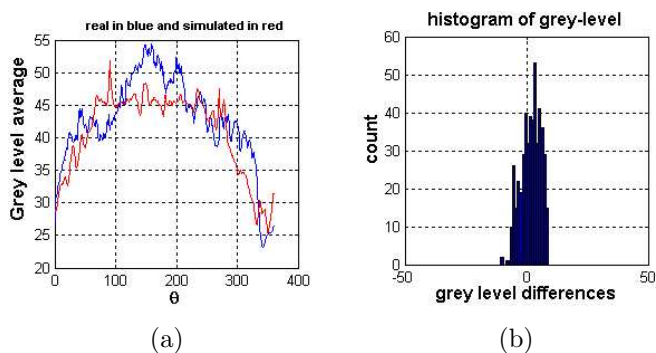


Figure 40: Global projections in direction θ (a), from Fig. 38 (b) and (d), the corresponding histogram grey level differences (b).

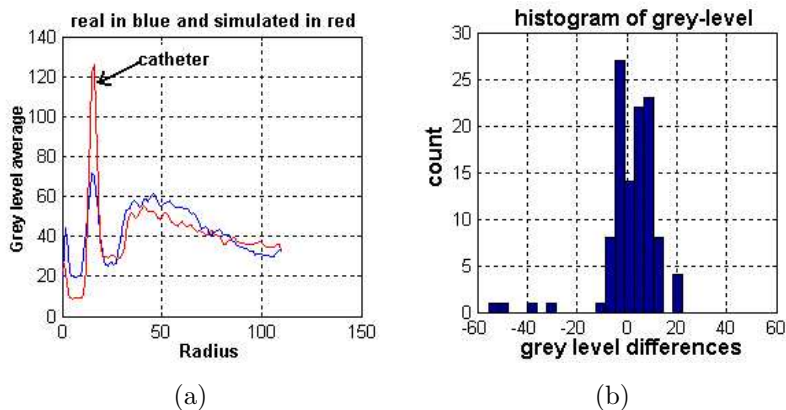


Figure 41: Global projection in R direction (c), from Fig. 38 (b) and (d), the corresponding histogram grey level difference are shown in (b).

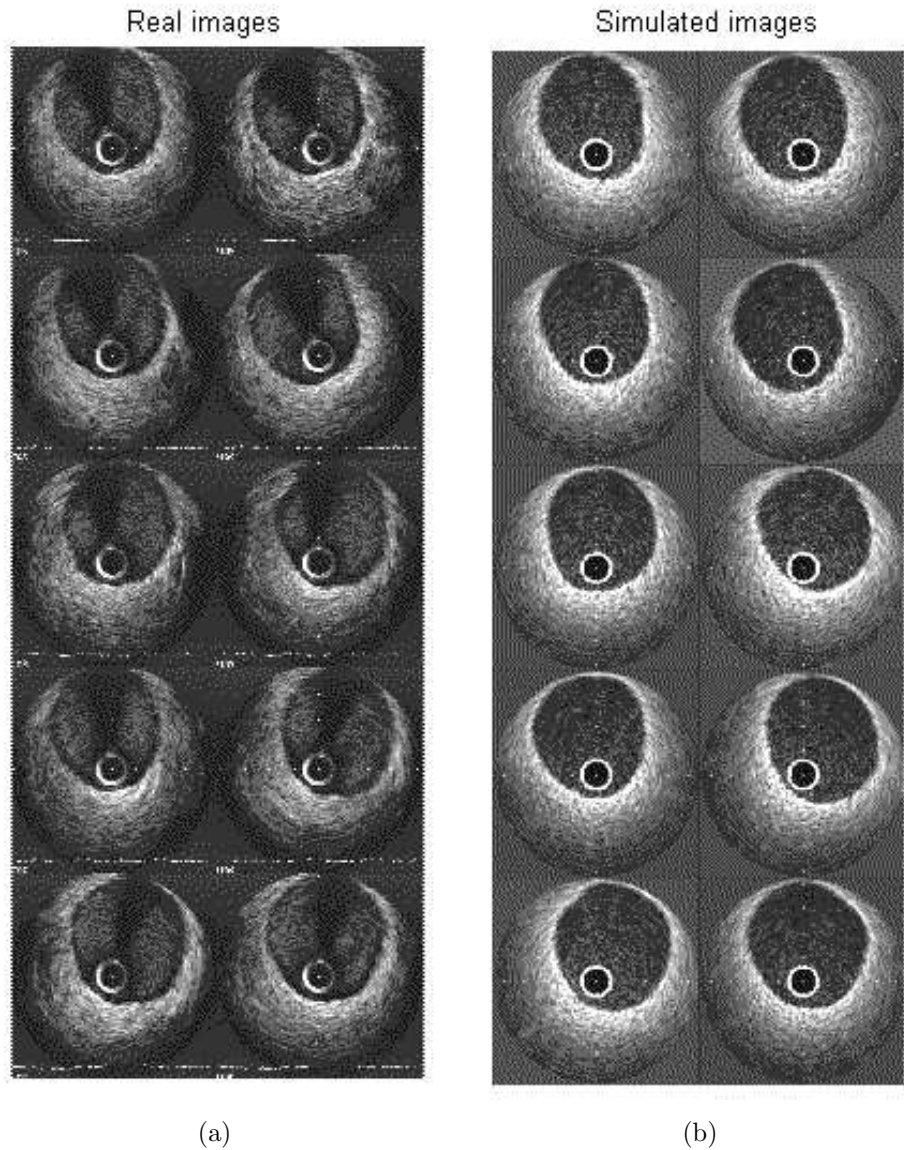
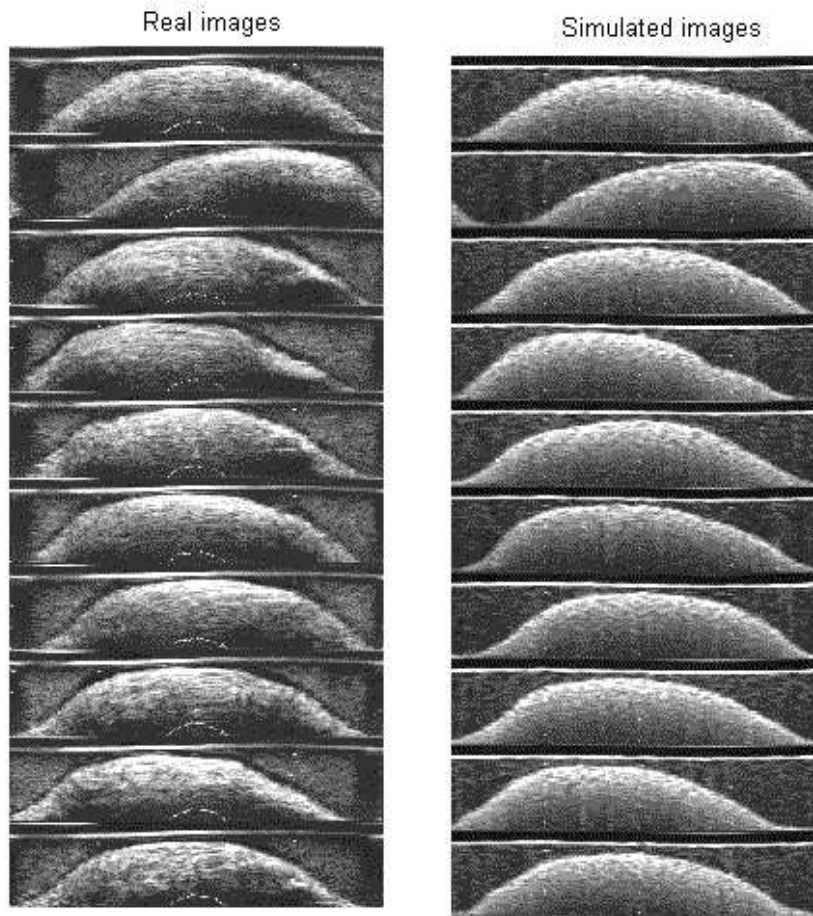


Figure 42: 10 original IVUS images (a) and the corresponding simulated (b) images.



(a)

(b)

Figure 43: 10 polar real images (a) and the corresponding simulated (b) images.

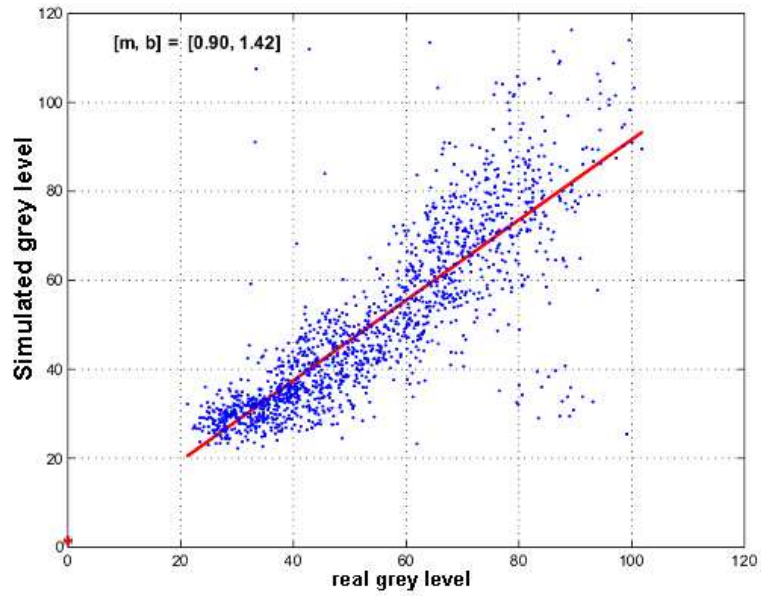


Figure 44: Simulated vs real gray level values for 20 ROIs comparing pixel grey level and the regression line.

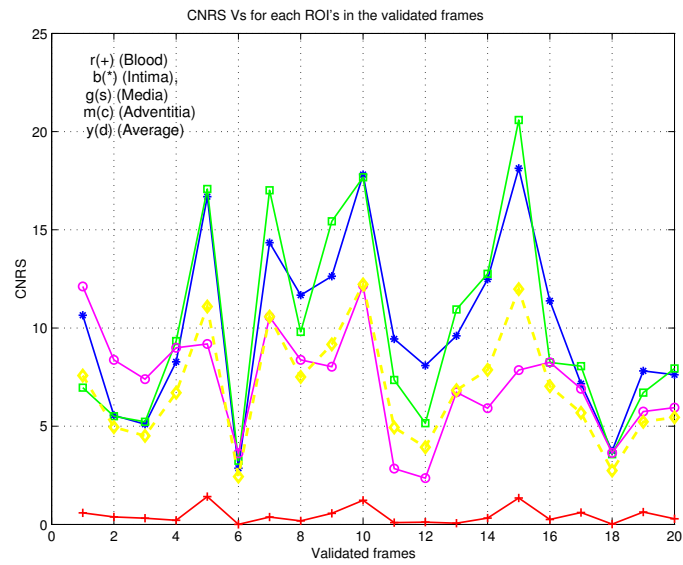


Figure 45: CNRS values for each ROIs of 20 manually segmented image frames.

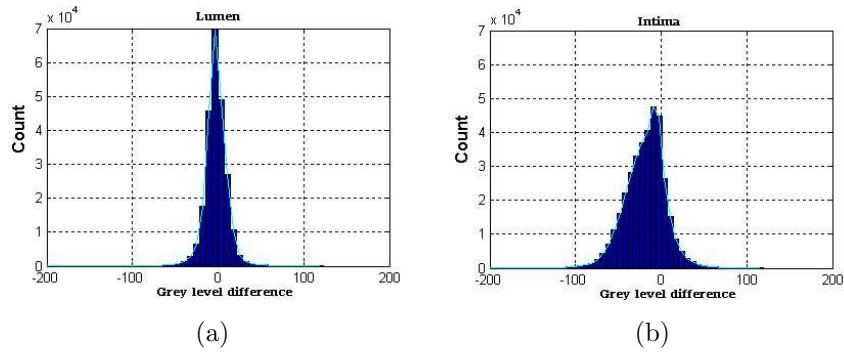


Figure 46: Histogram of grey level differences for lumen (a) and intima (b).

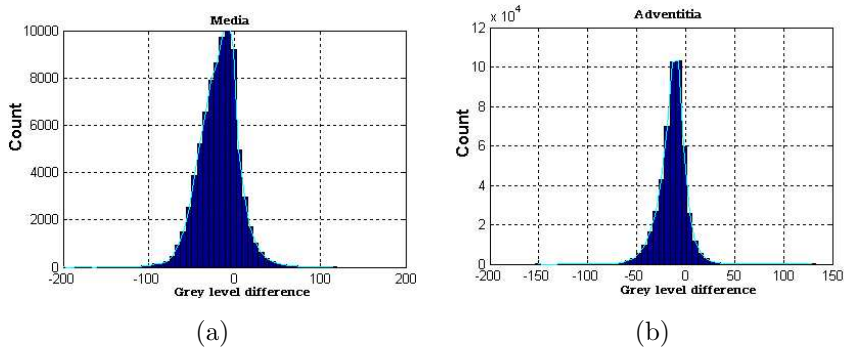


Figure 47: Histogram of grey level differences for media (a) and adventitia (b).

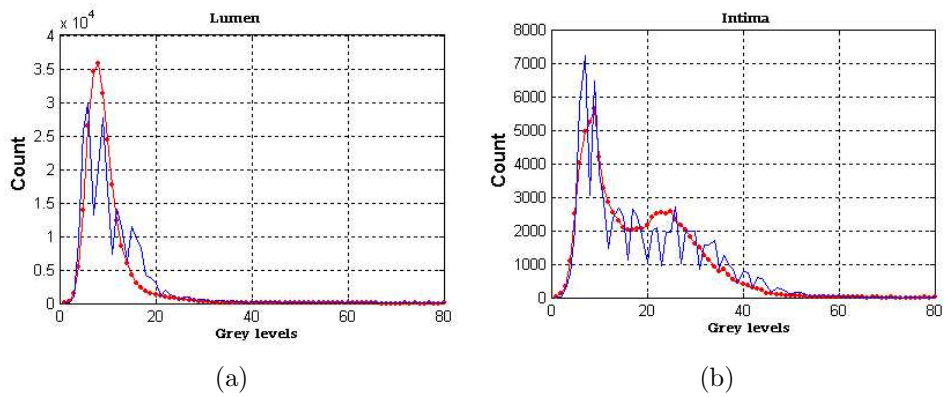


Figure 48: Real (in blue) and simulated (in red) grey level distributions for lumen (a) and intima (b)

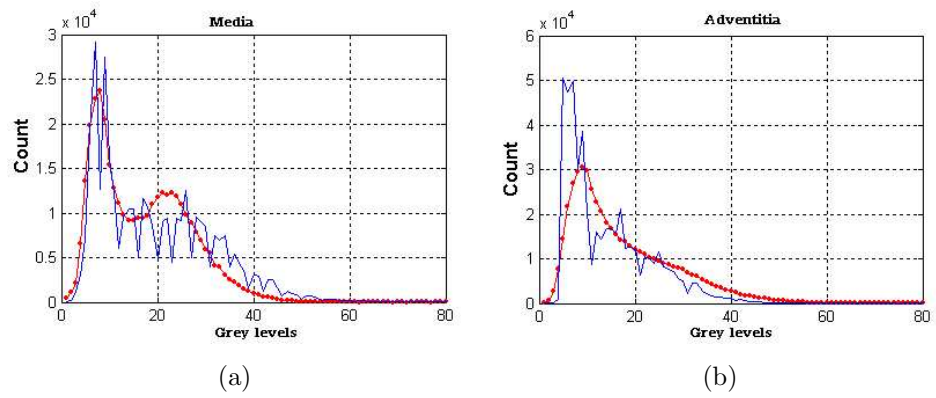


Figure 49: Real (in blue) and simulated (in red) grey level distributions for media (a) and adventitia (b)

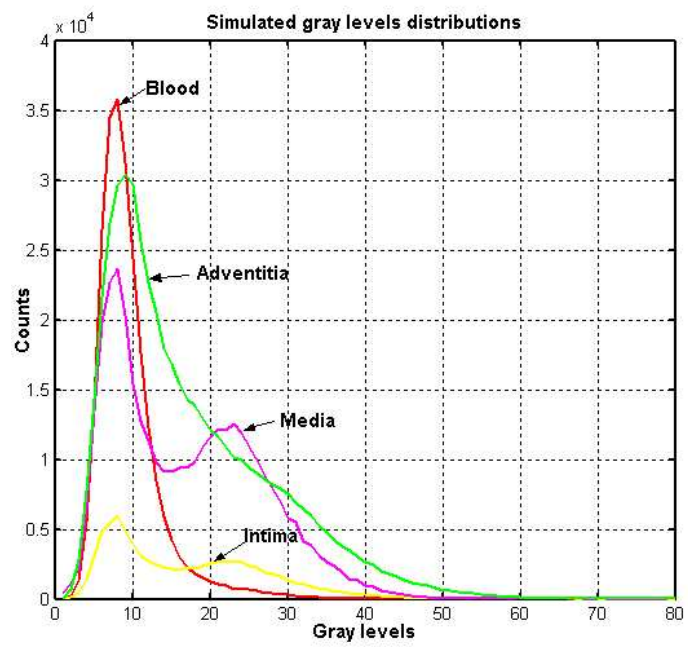


Figure 50: Simulated grey level distributions for blood, intima, media and adventitia.

Conclusions

0.7 Conclusions

Although IVUS is continuously gaining its use in practice due to its multiple clinical advantages, the technical process of IVUS image generation is not known by doctors and researchers developing IVUS image analysis. This fact leads to a simplified use, analysis and interpretation of IVUS images based only on the grey level values of image pixels.

In this chapter we discuss a basic physical model to generate synthetic 2D IVUS images. The model has different utilities: Firstly, expert can generate simulated IVUS images in order to observe different arterial structures of clinical interest and their grey level distribution in real images. Secondly, researchers and doctors can use our model to learn and to compare the influence of different physical parameters in the IVUS image formation, for example: the ultrasound frequency, the attenuation coefficient, the beam number influence, and the artifact generations. Third, this model can generate large database of synthetic data under different device and acquisition parameters to be used to validate the robustness of image processing techniques. The IVUS image generation model provides a basic methodology that allows to observe the most important real image emulation aspects. This initial phase does not have the intention to compare pixel to pixel values generation, showing the coincidence with the real image, but looks for a global comparison method based on gray level difference distribution. The input model applies standard parameters that have been extracted from the literature. Hence this model is generic in terms that the model allows simulating different processes, parameters, and makes possible to compare to real data and to justify the generated data from the technical point of view.

The model is based on the interaction of the ultrasound waves with a discrete scatterer distribution of the main arterial structures. The obtained results of the validation of our model illustrate a good approximation to the image for-

mation process. The 2D IVUS images show a good correspondence between the arterial structures that generate the image structures and their gray level values. The simulations of the regions and tissue transitions of interest lumen, lumen/intima, intima/media, media/adventitia and adventitia, have been achieved in a satisfactory degree. Interested readers are invited to check the generation model in (<http://www.cvc.uab.es/~misael>).

Bibliography

- [1] Ponte Ignacio C., La epidemia del siglo XXI. Director de la Sección de Cardiología preventiva del Hospital Dr. Domingo Luciani, <http://www.aventispharma.com.ve/cardio.htm>, El Llanito, Edo. Miranda Venezuela, 2003.
- [2] Metz J., Paul G., Fitzgerald P., Intravascular Ultrasound Imaging, Jonathan M. Tobis y Paul G. Yock. Churchill Livingstone Inc., 1992.
- [3] Yock P., Linker D., Saether O., et al., Intravascular two dimensional catheter ultrasound, Initial clinical studies, abstracted, Circulations, No. 78 (suppl II): II-21, 1988.
- [4] Graham S., Brands D., Sheehan H., et al., Assesment of arterial wall morphology using intravascular ultrasound in vitro and in patient, Circulations, (Suppl II): II-56, 1989.
- [5] Metz Jonas A., Paul G., Fitzgerald Peter J., Intravascular ultrasound basic interpretation, in Beyond Angiography, Intravascular Ultrasound, State of the art, Vol. XX, Congress of the ESC Viena-Austria, Stanford University School of Medicine, California, USA., 1998.
- [6] Jumbo G., Raimund E., Novel techniques of coronary artery imaging, in Beyond Angiography, Intra vascular Ultrasound, state of the art, Vol. XX, Congress of the ESC Viena-Austria, University of Essen,Germany, 1998.
- [7] Korte Chris L., Intravascular Ultrasound Elastography, Article compilation of its doctoral thesis, Interuniversity Cardiology Institute of the Netherlands (ICIN), 1999.
- [8] Kearney P., Erbel R., Imaging in the characterization laboratory, in Beyond Angiography, Intra vascular Ultrasound, state of the art, Vol. XX, Congress of the ESC Viena-Austria, Johannes Gutenberg University, Mainz and University Clinic,Essen,Germany, 1998.

- [9] Berry E., and et al, Intravascular ultrasound-guided interventions in coronary artery disease, Tech. Rep., Healt Technology Assesment, NHS R D HTA Programme. A systemac literature review, with decisions-analytic modelling, of outcomes and cot-effectiveness, 2000.
- [10] Verhoef W. A., Cloostermans M. J., Thijssen J. M., The impulse response of a focused source with an arbitrary axisymmetric surface velocity distribution, Journal Acoustic Society American, Vol. 75, pp. 1717-1721, 1984.
- [11] Fontaine I., Bertrand M, Cloutier G., A system-based approach to modelling the ultrasound signal backscattered by red blood cells,Biophysical Journal, Vol. 77, pp. 2387-2399, 1999
- [12] Fan L., Herrington D., Santiago P., Simulation of b-mode ultrasound to determine features of vessel for image analysis,Computers in Cardiology, Vol. 25, pp. 165-168,1998
- [13] Kinsler L. , Fundamentos de acústica, LIMUSA, Noriega Editores, 1995.
- [14] Cheeke D., Fundamentals and Aplications of Ultrasonic Waves, CRC PRESS, 2002.
- [15] Thijssen J, Oosterveld B., Perfomance of echographic equipment and potentials for tissue characterization, NATO ASI Series, Mathematics and Computer Science in Medical Imaging, Vol. F39, pp. 455-468, 1988.
- [16] Zagzebski J., Essential of Ultrasound Physics, Mosby A. hardcourt Healt Sciences Company, 1996.
- [17] Arendt Jesen J., Linear Descripcion of Ultrasound Imaging System, Notes for the international Summer School on Advanced Ultrasound Imaging, Tecnical University of Denamark, 2001.
- [18] Young B., and Heath J., Wheater's, Histología Funcional, 4ta edición, Ediciones Hardcourt, S.A, 2000. edicion.
- [19] Mazumdar J., Biofluids Mechanics, World Scientific Publishing, 1992.
- [20] Shung and Thieme., Ultrasonic scatering in biological tissues, CRC Press, Boca Raton, Ann Arbor, London,Tokyo, 1993.

- [21] Guyton A., Tratado de Fisiología Médica, Décima edición, Mcgraw-Hill Interamericana, 2001.
- [22] Perelman L., and et al, Observation of periodic fine structure in reflectance from biological tissue: A new technique for measuring nuclear size distribution, Physical Review Letters, Vol. 80, No. 3, pp. 627-630, January 1998.
- [23] Duda R., Hart P., Stork D., Pattern Clasification, Johon Wiley & sons, INC, 2000.
- [24] Boston Scientific Corporation, Scimed division, The ABCs of IVUS, 1998.
- [25] Gonzales R., Wintz P., Digital Image Processing, Addison Wesley, 1987.
- [26] O'Donnell M., Silverstein S., Optimum displacement for compound image generation in medical ultrasound, IEEE Transaction on Ultrasonics, Ferroelectrics and Frequency Control, Vol. 35, No. 4, pp. 470-476, 1988.
- [27] Rosales M., Radeva P., Empirical simulation model of intravascular ultrasound, Tech. Rep., No. 71, Centre de Visió per Computador, Universitat Autònoma de Barcelona/España, 2003.
- [28] Vogt M., and et al, Strutural analysis of the skin using high frequency broadband ultrasound in the range from 30 to 140 mhz, IEEE Internationalk Ultrasonics Syposium, Sendai, Japan, 1998.

Question and Answer

0.7.1 Questions

(Q1) Which qualitative phenomenon and parameters are possible to be observed using IVUS technique ?

(Q2) Which principles is IVUS data acquisition based on ?

(Q3) What are the principal limitations of the IVUS technique ?

(Q4) How is the distance to reflecting object by ultrasound technique determined ?

(Q5) What is the attenuation coefficient ?

(Q6) What are the axial and radial resolution ?

(Q7) What is the usual IVUS resolution ?

(Q8) How many scatterers structures are taken into account by a basic IVUS image model ?

(Q9) How are the 1D and 2D echograms generated ?

(Q10) What are the steps followed in the generation of an IVUS image ?

0.7.2 Answers

(A1) The introduction in the field of the medical image of the **IntraVascular UltraSound (IVUS)** as an exploratory technique has made a significant change to the understanding of the arterial diseases and individual patterns of diseases in the coronary arteries. IVUS technique visualizes the cross-section of the artery allowing an evaluation of the plaque as well as of the different layers from the arterial wall. The IVUS image provides qualitative information about: The causes and severity of the narrowing of the arterial lumen, distinction of thrombus of the arteriosclerotic plaque, recognition of calcium deposits in the arterial wall, unexpected evaluation of the awaited changes and complications in the coronary arteries after an intervention as angioplasty, evaluation and diagnose of coronary arterial aneurysms, diagnose of fissures of arterial coronary plaques: determination and location, dimensions, type (eccentric and concen-

tric) and composition of the arteriosclerotic plaque.

(A2) The IVUS technique is based on the reception and transmission of the high frequency sound waves. The transmitted wave propagates through the material until striking the reflecting object. The reflected wave returns and is received by the pivoting transducer. The time between the transmission and the reception of the wave is directly related to the distance between the source and the reflector. A standard configuration of IVUS acquisition images consists of three components: A catheter with a piezoelectric transducer miniaturized, the pull-back unit and the console to reconstruct the images. IVUS catheter has a range of measures that oscillates between 2,9 to 3,5 F (0,96 to 1,17 mm) of diameter. The quality of the image depends on the operation frequency, being this of the order of 20 to 50 Mhz, the lateral resolution is approximately of order of 113 μm and the axial resolution is of order of 80 μm . The IVUS image acquisition process, is initiated when the catheter is manually (guided by the angiography) inserted within the artery. The catheter pullback is made at linear constant velocity (usually 0.5 mm/s), and constant angular velocity of 1800 rev/min. The pivoting transducer sends a radially focused beam of ultrasound and receives its corresponding echoes. The obtained radial lines for different transducer angular positions are adequately processed, giving as a result a 2D cross section artery image. The sequence can be shown as a longitudinal sequence, which gives a longitudinal artery cut. The resolution of a ultrasound image is directly related to the ultrasound signal frequency, high frequencies allow to obtain better resolution. Nevertheless, increasing the frequency, the attenuation of the waves of ultrasound increases while penetrating the biological tissue. The typical frequencies of IVUS technique are in the range from 20 to 50 MHz, allowing to obtain inferior resolutions of 50 μm .

(A3) The precision in the measurements of distance by the IVUS technique are subject to the following potential sources of error: a) Incorrect identification of the surface and the sections to be measured, b) Assumption that the sound speed is constant in the arterial structure, which brings as a consequence the propagation of the error to the location of each one of the structures in study. c) Artifacts caused by inhomogeneities in the rotation of the catheter and pronounced reverberations generated by very acute irregularities of the vessel. f)

Presence of zones of acoustic shade which prevents to access certain regions of interest, g) The presence of the catheter, the reticule and the guide leading to troublesome for the processing of the images. h) Impossibility of catheter spatial location. The impossibility to locate the catheter with respect to a specific axis of coordinates makes impossible any attempt of three-dimensional representation of the vessel only with IVUS technique, i) Impossibility to evaluate dynamic parameters, different from the single static characterization using the grey levels.

(A4) The determination of the distance D between the emitter/receiver and the reflecting object is done from the difference of time between the transmitted pulse P_o and the received pulse P_1 assuming that the pulse speed c is constant.

(A5) The **attenuation coefficient**, α gives the rate of diminution of average power with respect to the distance along a transmission path. It is composed of two parts, one (absorption) proportional to frequency, the other (scattering) dependent on the ratio of grain, particle size or the scatterers number located along the ultrasound beam path. Since the attenuation is frequency dependent, a single attenuation coefficient only applies to a single frequency. The attenuation coefficient of ultrasound is measured in units of dB/cm. In biological soft tissues, the ultrasound attenuation coefficient is roughly proportional to the ultrasound frequency (for the frequency range used in medical imaging). This means that the attenuation coefficient divided by the frequency (unit $dB/MHz \times cm$) is nearly constant in a given tissue. Typical soft tissue values are 0.5 to 1.0 $dB/MHz \times cm$.

(A6) a) The **axial resolution** is the capacity that the ultrasound technique has to separate the spatial position of two consecutive scatterers through its time corresponding echoes or temporary delay. The axial resolution of this technique depends essentially on two factors: The ultrasound speed c and pulse duration d_t . The functional dependency between the spatial resolution, the frequency and the ultrasound speed propagation, is given by: $d_r = \frac{c}{f}$, where c is the ultrasound speed for biological tissues and f is the ultrasound frequency. b) The **angular resolution** is the capacity to discern two objects or events located in the tangential direction and depends on the beam width. The tangential or lat-

eral resolution of a ultrasound emitter of diameter, D that emits by frequency f is given by: $d_\theta = 1.22 \frac{\lambda}{D}$, where $\lambda = c/f$ and D is the transducer diameter.

(A7) The axial resolution at frequency of 30 MHz is approximately: $d_r = 1540/(30 \times 10^6) = 0.05 \text{ mm} \approx 50 \mu\text{m}$ and the typical lateral resolution is $d_\theta \approx 0.10^{\text{a}}$.

(A8) The scatterers structures to be simulated can be classified in 3 groups: Tissue structures, non tissue structures and artifacts. The tissue scatterers, are determined by the contribution of the normal artery structure, corresponding to: lumen, intima, media and adventitia. Non tissue scatterers, these contributions can be originated by structures formed by spatial calcium accumulation, which are characterized because the density is greater than the rest of the arterial structure. Artifacts scatterers are caused by the sheathing transducer.

(A9) To obtain an **1D echogram**, a ultrasound pulse is emitted by the transducer. The pulse moves axially through scatterers, its intensity distribution decreases with the penetration depth and the scatterers numbers on the ultrasound way. The echoes amplitude is registered by the transducer as a signal function of time $S(t)$. The value is transformed to penetration depth replacing $t = x/c$ and normalized to grey scale. The procedure to obtain the **2D IVUS echogram** is the following: A rotatory transducer at angular velocity, ω is located at the center of the simulated arterial configuration. The transducer emits a ultrasound pulse radially focused at frequency, f_o along angular direction, θ_1 . The pulse progressively penetrates each one of the layers of the simulated arterial structure. Each one of the layers generates a profile of amplitude or echoes in the time, that can be transformed into a profile of amplitude as a function of the penetration depth. This procedure is made n-times for the angles, $(\theta_1, \dots, \theta_n)$ and the 2D image is generated.

(A10) The procedures to obtain the final IVUS simulated image is as follows: 1) The echoes are obtained by the pivoting transducer. 2) Each echo profile is assigned at the corresponding angular position. 3) The original image is transformed to a polar form. 4) Secondary beams are computed between two original neighbor beams. 5) The image is smoothed by a 2×2 median filter. 6)

The image is again transformed to cartesian form. As a result of this transformation, a significant number of pixel is empty. 7) The empty pixels are filled in a recursive way, using for this an average of the eight nearest neighbors. 8) An image reference reticle is added and a gaussian filter is applied.